MRI of Rhabdomyosarcoma and Other Soft-Tissue Sarcomas in Children

Emilio J. Inarejos Clemente, MD
María Navallas, MD
Ignasi Barber Martínez de la Torre, PhD
Mariona Suñol, MD
Josep Munuera del Cerro, PhD
Ferran Torner, MD
Moira Garraus, MD
Oscar M. Navarro, MD

Soft-tissue sarcomas in children comprise a heterogeneous group of entities with variable manifestation depending on the age of the patient and the location of the tumor. MRI is the modality of choice for evaluating musculoskeletal soft-tissue tumors and plays a paramount role in both initial diagnosis and assessment of tumor response during and after treatment. Conventional MRI sequences, such as T1- and T2-weighted imaging, offer morphologic information, which is important for localizing the lesion and describing anatomic relationships but not accurate for determining its malignant or benign nature and may be limited in differentiating tumor response from therapy-related changes. Advanced multiparametric MRI offers further functional information that can help with these tasks by using different imaging sequences and biomarkers. The authors present the role of MRI in rhabdomyosarcoma and other soft-tissue sarcomas in children, emphasizing a multiparametric approach with focus on the utility and potential added value of diffusion-weighted imaging (DWI) and dynamic contrast-enhanced MRI in characterization and staging, determination of pretreatment extent, and evaluation of tumor response and recurrence after treatment.

Abbreviations: ADC = apparent diffusion coefficient, DCE = dynamic contrast-enhanced, DWI = diffusion-weighted imaging, MPNST = malignant peripheral nerve sheath tumor, NF1 = neurofibromatosis type 1, TIC = time-intensity curve

RadioGraphics 2020; 40:0000–0000

https://doi.org/10.1148/rg.2020190119

Content Codes: MR OI PD

From the Departments of Diagnostic Imaging (E.J.I.C., M.N., I.B.M.d.l.T., J.M.d.C.), Pathology (M.S.), Orthopaedics (F.T.), and Oncology and Haematology (M.G.), Hospital Sant Joan de Déu, Av Sant Joan de Déu 2, 08950 Esplugues de Llobregat (Barcelona), Spain; Department of Medical Imaging, University of Toronto, Toronto, Ont, Canada (O.M.N.); and Department of Diagnostic Imaging, Hospital for Sick Children, Toronto, Ont, Canada (O.M.N.). Presented as an education exhibit at the 2018 RSNA Annual Meeting. Received April 17, 2019; revision requested July 24 and received September 4; accepted September 13. For this journal-based SA-CME activity, the author J.M.d.C. has provided disclosures (see end of article); all other authors, the editor, and the reviewers have disclosed no relevant relationships. **Address correspondence to** E.J.I.C. (e-mail: *emilioinarejos@gmail.com*).

SA-CME LEARNING OBJECTIVES

After completing this journal-based SA-CME activity, participants will be able to:

- Describe conventional and multiparametric MRI techniques used in children with soft-tissue sarcomas.
- List the most frequent manifestations of soft-tissue sarcomas in children at conventional and multiparametric MRI.
- Discuss use of multiparametric MRI for diagnosis of soft-tissue sarcomas in children, follow-up during and after treatment, and evaluation of residual disease after surgery.

See rsna.org/learning-center-rg.

Introduction

Soft-tissue sarcomas comprise a diverse group of more than 50 different histologic tumors of presumed mesenchymal origin, with a wide range of biologic and clinical behavior varying from less aggressive to highly malignant (1). Soft-tissue sarcomas are infrequent neoplasms, with an annual incidence of around five or six cases per 100 000, and account for about 1% of all malignant tumors, which represents 7% of all pediatric malignancies (1,2).

Soft-tissue sarcomas have variable clinical and imaging manifestations depending on the age of the patient, the location of the tumor, and the content of the tumor. Imaging is necessary at the time of initial diagnosis and as part of evaluation of tumor response after treatment.

Owing to its contrast resolution, MRI is the modality of choice for evaluation and characterization of soft-tissue sarcomas, which are achieved by combining conventional and advanced multiparametric MRI (3). Conventional MRI techniques can demonstrate tumor composition, extent, compartmental involvement, and relationship with other structures for accurate treatment planning before surgery. However, conventional techniques remain inadequate for differentiation of malignant from benign lesions owing to overlap in the signal intensity characteristics of these tumors and are also limited in assessment of residual or recurrent disease after treatment (3,4).

Traditionally, assessment of tumor response in soft-tissue sarcomas has been achieved by using three-dimensional measurements (based on the European Pediatric Soft-Tissue Sarcoma Study Group [EpSSG] guidelines) and more recently by using one-dimensional

TEACHING POINTS

- Volumetric determination of tumor ADC (ADC histogram analysis) has become more reproducible and a better reflector of lesion heterogeneity than cross-sectional analysis of a single region of interest (ROI), which may cause selection bias.
- A type I profile is associated with necrosis or a cystic component, type II with benign processes, types III and IV with malignancy, and type V with granulation tissue or fibrosis.
- Soft-tissue sarcomas generally manifest with fast enhancement and higher slopes of arterial enhancement than benign lesions, although this pattern is not entirely specific and has to be evaluated together with results from DWI and anatomic sequences.
- Whole-lesion ADC histogram analysis of embryonal rhabdomyosarcoma does not usually demonstrate restriction as a consequence of internal necrosis and myxoid component.
- At MRI, triple signal intensity in a soft-tissue mass has been described as a highly suggestive sign of synovial sarcoma.

measurements (based on the Response Evaluation Criteria in Solid Tumors [RECIST]). However, both of these methods should be used with caution, as their interobserver and intermethod variability can result in different treatment options (5).

Multiparametric or functional MRI, which includes techniques such as diffusion-weighted imaging (DWI), chemical shift imaging, and dynamic contrast-enhanced (DCE) MRI, can allow more accurate characterization of malignancy, assessment of treatment response, and evaluation of postsurgical residual or recurrent disease (Table 1).

Multiparametric MRI does not replace conventional MRI. It is important to perform a combined analysis of the information provided by conventional sequences (T1- and T2-weighted imaging) together with functional sequences, because each may provide some additional value in evaluation of a soft-tissue tumor, including characterization, determination of extent, and assessment of response during and after treatment (4,6). In the future, multiparametric MRI may play a paramount role in assessment of tumor response and complement the currently used measurement-based guidelines.

Histologic findings, which are obtained with percutaneous or surgical biopsy, are the reference standard for final diagnosis and tumor grading.

In this article, we review the epidemiologic features, clinical features, histopathologic findings, and conventional MRI and multiparametric MRI characteristics—with emphasis on DWI and DCE MRI—of rhabdomyosarcoma and other less common soft-tissue sarcomas in children, including malignant peripheral nerve sheath tumor (MPNST), synovial sarcoma, extraosseous Ewing sarcoma, infantile fibrosarcoma, epithelioid sarcoma, and extrarenal rhabdoid tumor. Treatment of and prognosis for these tumors and posttreatment imaging are also discussed.

MRI Protocol

The MRI protocol is based on a combination of anatomic and multiparametric sequences to adequately evaluate soft-tissue sarcomas (4,7). Each sequence provides complementary information for evaluation of a tumor, including characterization, extension, and response assessment after treatment. Table 2 shows the protocol used at our institution.

Conventional MRI

Soft-tissue sarcomas do not have a specific MRI pattern, showing variable signal intensity on T1- and T2-weighted images (4). The appearance with these sequences varies depending on the presence of hemorrhage, necrosis, or myxoid change (4,8,9). Conventional T1-weighted and fluid-sensitive MRI sequences (fat-suppressed T2-weighted or short τ inversion-recovery [STIR]) are important for identifying and delineating the extent of a tumor.

Soft-tissue sarcomas are usually isointense to muscle on T1-weighted images, with variable degree of hyperintensity to muscle on fluid-sensitive images (10). Newer fluid-sensitive sequences, such as spectral presaturation with inversion recovery (SPIR) and Dixon sequences, produce more homogeneous suppression of fat and provide better contrast between fluid and surrounding tissues compared with traditional STIR or fat-suppressed T2-weighted images (11).

Multiparametric MRI

Diffusion-weighted Imaging.—DWI provides quantitative functional information on tumor cellularity, helping in differentiation between benign and malignant entities as well as improving MRI evaluation of treatment response (3,4,12,13). DWI is considered useful in assessing treatment response sooner than conventional imaging (4).

Mean apparent diffusion coefficient (ADC) values may help differentiate benign and malignant lesions, whereas changes in ADC tumor heterogeneity evaluated longitudinally during treatment may provide another method of characterizing tumor viability. A precondition for such evaluation is a uniform repeatable method of analyzing sufficient tumor volume so that all parts of the tumor, both necrotic and solid, are included (14,15).

Volumetric determination of tumor ADC (ADC histogram analysis) has become more reproducible and a better reflector of lesion heterogeneity than cross-sectional analysis of a single region of interest (ROI), which may cause selection bias (16). Whole-lesion ADC histogram

Table 1: Multiparametric MRI Techniques and Type of Information Provided

Multiparametric MRI Technique	Type of Information Provided
DWI	Cellularity
DCE imaging	Vascularization
Chemical shift imaging	Fat
MR spectroscopy	Metabolism

Table 2: MRI Protocol for Study of Soft-Tissue Sarcomas with a 3.0-T Imaging Unit

Sequence	No. of Sections	FOV (mm)	Voxel Size (mm)	Section Thickness/ Gap (mm)	TR/TE (msec)	NSA	Flip Angle (degrees)	TA (min:sec)
Coronal T2W Dixon	52	320	0.6 × 0.7	1.5/0	3300/60	1.0	90	2:34
Coronal T1W TSE	52	320	0.8 × 0.8	1.5/0	700/10	1.0	90	3:03
Sagittal T2W Dixon	52	300	0.6 × 0.7	1.5/0	3200/60	1.0	90	2:38
Sagittal T2W FFE	52	300	0.6 × 0.7	1.5/0	575/12	1.0	20	1:57
Axial T2W Dixon	60	120	0.6 × 0.7	3.0/0	3600/60	1.5	90	2:48
Axial T1W TSE	60	120	0.5 × 0.6	3.0/0	700/10	1.0	90	2:09
Axial DWI*	60	120	1.1 × 1.1	3.0/0	9000/78	2.0	90	4:06
THRIVE T1W TFE	75†	300	1.5 × 1.5	1.5/0	4/2	1.0	10	5:08
Sagittal T1W FS + CE	52	300	0.8 × 0.8	1.5/0	600/10	1.0	90	2:19
Axial T1W FS + CE	60	120	0.5 × 0.6	3.0/0	700/10	1.0	90	3:28

Note.—CE = contrast-enhanced, FFE = fast field echo, FOV = field of view, FS = fat-suppressed, NSA = number of signals acquired, TA = acquisition time, TE = echo time, TFE = turbo field echo, THRIVE = T1-weighted high-resolution isotropic volume examination, T1W = T1-weighted, TR = repetition time, TSE = turbo spin-echo, T2W = T2-weighted.

*b value = 0, 500, and 800 sec/mm^2.

†Thirty series after administration of contrast material.

analysis has been used to distinguish benign from malignant neoplasms in different organs and is reported to allow differentiation of tumor grades and prediction of therapeutic response in patients with different types of tumors (16,17).

With regard to predicting therapeutic response, ADC histogram analysis has to be performed before, during, and after treatment. Tumor response assessment needs to be correlated with the displacement of the histogram through the x axis. Good treatment response increases the ADC of the tumor; thus, there is displacement of the histogram to the right of the graph. However, in cases where the tumor is not responding, there is overlap or no displacement of the histogram through the x axis of the graph (17,18).

Perfusion MRI.—Perfusion MRI comprises both sequences that do not require use of intravenous contrast material, such as DWI, and sequences that are performed after intravenous administration of contrast material, such as DCE MRI, which is currently the most used technique.

It is highly recommended that one perform a temporal resolution acquisition of less than 5 seconds for 4–5 minutes (4,19,20), called TRICKS (time-resolved imaging of contrast kinetics) or TRAK (time-resolved MR angiography with keyhole), depending on the vendor. Analysis of DCE MRI data can be performed by using a variety of postprocessing techniques and creating time-intensity curves (TICs) from an ROI (21).

A qualitative analysis approach relies on TICs or the curve profile. Studying the pattern of enhancement over time with a TIC is not only useful for diagnosis but also helpful for treatment, as it offers information on the vascular pharmacokinetics of soft-tissue sarcomas (19).

There are different classifications of TIC profiles. van Rijswijk et al (22) described five types of curve profiles in synovial sarcoma; these can be extrapolated to other soft-tissue tumors (Fig 1). A type I curve shows lack of enhancement, resulting in a horizontal curve; type II shows progressive enhancement; type III shows a delayed plateau; type IV shows delayed washout; and type

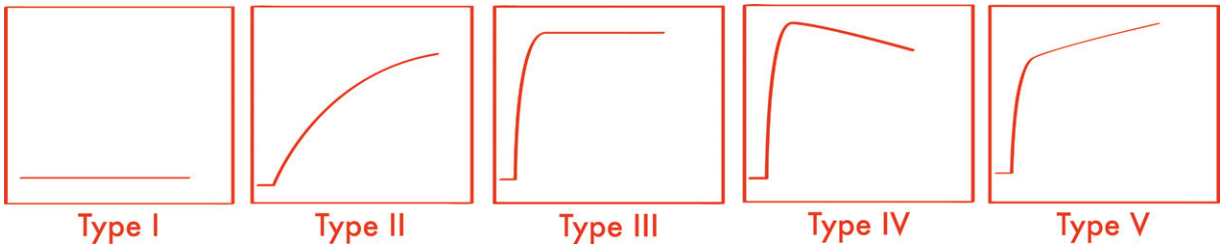

Figure 1. TIC profiles from DCE MRI. Type I is associated with necrosis. Type II has typically been associated with benign conditions. Types III and IV have been linked to malignancy. Type V is associated with granulation tissue or fibrosis. (Adapted and reprinted, with permission, from reference 21.)

V shows rapid initial enhancement followed by sustained late enhancement. A type I profile is associated with necrosis or a cystic component, type II with benign processes, types III and IV with malignancy, and type V with granulation tissue or fibrosis (22).

The slope of these curves indirectly reflects changes in tumor vascularization and therefore indicates the viability of the tumor. Curves with a steeper slope are seen in the vascularized portion, whereas a gradual slope is typical in an area of granulation tissue or fibrosis. DCE MRI helps in differentiation between regions of necrosis, viable tumor, granulation tissue or fibrosis, and blood vessels, as they manifest with different types of TICs (21).

Some benign tumors in the soft tissues may show features at conventional MRI that are indistinguishable from those of a sarcoma. In this setting, DCE MRI may reveal a type II curve profile with progressive enhancement, which may suggest a benign nature (Fig 2). Soft-tissue sarcomas generally manifest with fast enhancement and higher slopes of arterial enhancement than benign lesions, although this pattern is not entirely specific and has to be evaluated together with results from DWI and anatomic sequences (20,22).

TIC shape analysis does not provide absolute measurements and it is partly dependent on the protocol chosen. The length of the DCE MRI acquisition, the time resolution, and the imaging parameters (repetition time, flip angle) may all affect the final shape of the curve (21,22).

After completion of the DCE MRI study, it is recommended that a delayed contrast-enhanced fat-suppressed T1-weighted sequence be performed, which is one of the key components in differentiating solid tumors from cysts, delineating the margins of the mass, and estimating the amount of tumor necrosis (4).

Combination of anatomic sequences (T1-weighted, T2-weighted, and delayed contrast-enhanced) together with functional MRI (DWI and DCE imaging) provides detailed information on soft-tissue sarcomas at presentation and for assessment of treatment response (Table 3).

Soft-Tissue Sarcomas in Children

Rhabdomyosarcoma

Rhabdomyosarcoma is an aggressive tumor that can arise in almost any part of the body, with the exception of bone, and is thought to develop from primitive mesenchymal cells, most likely linked to skeletal muscle embryogenesis (23).

The imaging features are diverse owing to its different histologic subtypes, primary sites, and ages of presentation (24).

Rhabdomyosarcoma is the most common soft-tissue sarcoma in children and accounts for 4.5% of all pediatric malignancies (2). The annual incidence in the United States is four to five cases per million in children and adults younger than 20 years (2,24). Overall, it is the fourth most frequent solid tumor in childhood and the third most common pediatric extracranial solid tumor after neuroblastoma and Wilms tumor (2,24).

Rhabdomyosarcoma often develops in early childhood, with a median age at diagnosis of 5 years (2). There are three major histologic types: *(a)* embryonal rhabdomyosarcoma, which accounts for approximately 75% of cases; *(b)* alveolar rhabdomyosarcoma, which accounts for 20% of cases; and *(c)* pleomorphic rhabdomyosarcoma, which accounts for approximately 5% of cases and is exclusive to the adult population. Features of these types of rhabdomyosarcoma are given in Table 4 (23).

Genetic conditions associated with rhabdomyosarcoma include Beckwith-Wiedemann syndrome, Li-Fraumeni syndrome, pleuropulmonary blastoma, and some RASopathies, which are syndromes caused by germline mutations in genes that encode components or regulators of *RAS* genes. These disorders include, among other entities, neurofibromatosis type 1 (NF1), Costello syndrome, and Noonan syndrome (25,26). There is also a higher incidence of rhabdomyosarcoma in patients with retinoblastoma treated with radiation (27).

Rhabdomyosarcomas are locally aggressive secondary to their rapid growth. Affected children may also present with signs of compression or mass effect on surrounding structures, as rhabdomyosar-

Figure 2. Myofibroma involving the right thigh in a newborn. **(a)** Axial fat-suppressed T2-weighted image shows a heterogeneously hyperintense and lobulated mass (arrow) in the right vastus lateralis muscle. The mass has a central hyperintense area (*), which may represent necrosis. **(b, c)** Axial diffusion-weighted image **(b)** and corresponding ADC image **(c)** show restricted diffusion at the periphery of the mass (arrow) and T2 shine-through in the central area (*). **(d)** Left: DCE image shows heterogeneous enhancement of the mass (arrow). Right: Graph shows a type II TIC profile (arrow), which is usually seen in benign processes.

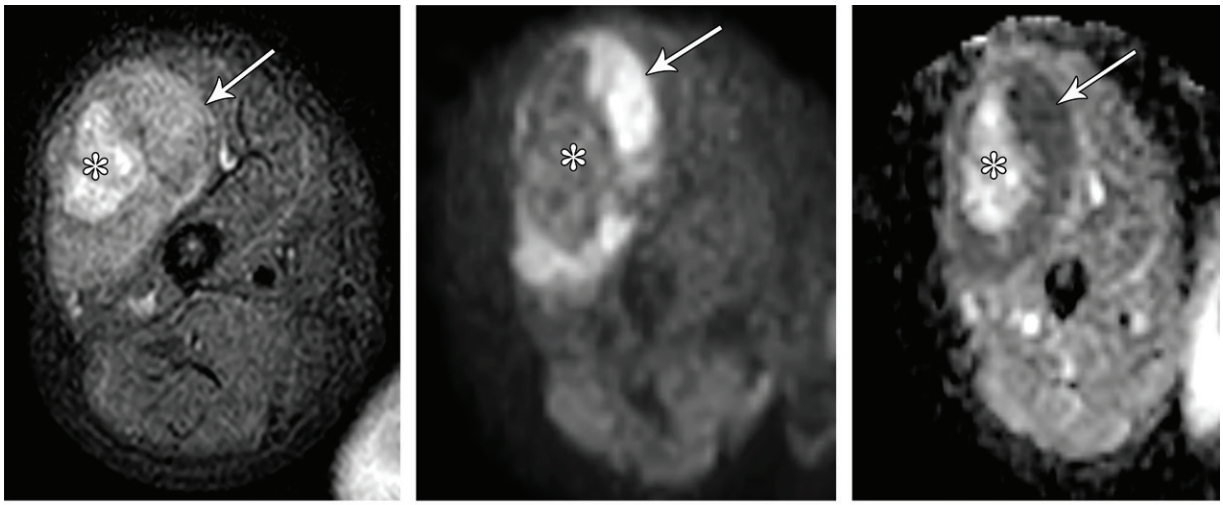

a. b. c.

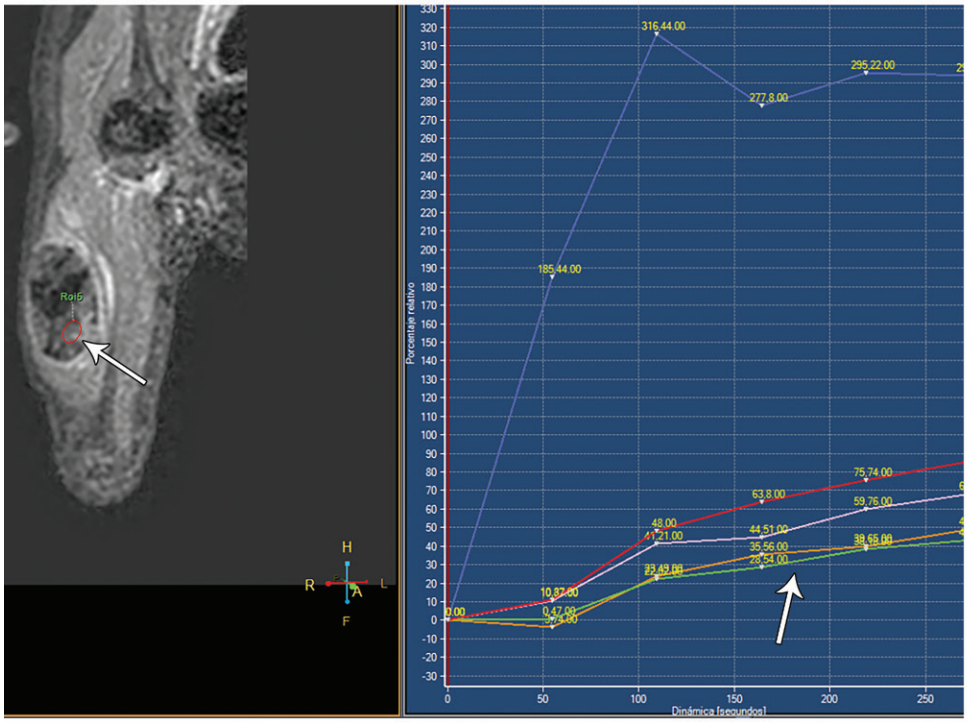

d.

comas tend to involve the neurovascular bundle and have a predilection for bone infiltration (23,24).

Embryonal Rhabdomyosarcoma

Epidemiologic Features.—The head and neck are the most common sites of involvement of this tumor type, accounting for 50% of all rhabdomyosarcomas (Table 5). The tumors can be parameningeal (50%), nonparameningeal (20%), or periorbital (25%) in location (24,28). Parameningeal rhabdomyosarcoma has the worst prognosis among the head and neck rhabdomyosarcomas, with 50% long-term survival.

The second most common location for this type of rhabdomyosarcoma is the genitourinary system (24). The botryoid variant is the most common variant of embryonal rhabdomyosarcoma arising in the pediatric genitourinary tract, including the bladder, prostate, and vagina. The name refers to the gross appearance, which resembles a bunch of grapes (*botryoid* in Greek) (29).

Table 3: Qualitative MRI Features of Biologic Processes Involved in Soft-Tissue Sarcomas

	MRI Appearance				
Biologic Process	T2W	T1W FS + CE	Diffusion Restriction	ADC	Type of DCE Curve Profile
Viable tumor	Isointense	Hyperintense	Increased	Decreased	III, IV
Granulation tissue	Hyperintense	Hyperintense	Increased	Increased	II, V
Fibrosis	Hypointense	Hypointense	Increased	Increased	II, V
Necrosis	Hyperintense	Hypointense	Increased	Increased	I

Note.—CE = contrast-enhanced, FS = fat-suppressed, T1W = T1-weighted, T2W = T2-weighted.

Table 4: Clinical Features of Histologic Types of Rhabdomyosarcoma

Histologic Type and Subtype	Prevalence (%)	Age Group	Prognosis	Location
Embryonal				
Spindle cell	50–70	<10 y	Good	Paratesticular, head and neck, retroperitoneum
Botryoid	50–70	<10 y	Good	Bladder, prostate, vagina, biliary tree
Alveolar	20	Infancy or adolescence	Poor	Extremities, trunk
Pleomorphic	5–10	Adults (>40 y)	Poor	Extremities (commonly thigh)

Botryoid rhabdomyosarcoma of the biliary tree is the most common malignant tumor of the biliary tract in children (30,31).

Clinical Features.—Clinical features are diverse and depend on the location of origin. Tumors arising in the head and neck usually manifest as proptosis, ophthalmoplegia, cranial nerve palsy, or meningeal symptoms (28).

Tumors arising in the urinary tract usually manifest as hematuria owing to intraluminal growth, whereas tumors involving the prostate or vagina tend to show signs and symptoms secondary to compression of surrounding structures (5,29).

Botryoid rhabdomyosarcoma of the biliary tree manifests as jaundice, pruritus, or abdominal distention (30,31).

The retroperitoneum and paratesticular region are other common sites of involvement by embryonal rhabdomyosarcoma. Retroperitoneal tumors typically manifest as an incidental abdominal mass, whereas paratesticular tumors tend to manifest as swelling of the scrotum or a well-defined solid mass in the scrotum, with variable degree of involvement of the testis (Fig 3) (32).

Histopathologic Findings.—Embryonal rhabdomyosarcoma arises from undifferentiated mesenchyme, which displays features of embryonic skeletal myogenesis. It is composed of primitive poorly differentiated mesenchymal cells with different patterns (23,32). Nuclear expression of MyoD1 and myogenin is characteristic and highly specific for rhabdomyosarcoma.

Conventional MRI Findings.—Embryonal rhabdomyosarcoma in the neck is typically a large and heterogeneous mass associated with regional lymphadenopathy (Fig 4). The mass is typically iso- to hyperintense to muscle on T1-weighted images and heterogeneously hyperintense to muscle on T2-weighted images owing to hemorrhage or necrosis (5) (Table 6). It shows inhomogeneous enhancement after contrast material injection (5,24).

Parameningeal rhabdomyosarcoma often manifests as a heterogeneous mass, with solid components alternating with large areas of fluid signal intensity that are hyperintense on T2-weighted images (33). The heterogeneity is secondary to internal necrosis or myxoid component, which correlates with high signal intensity on T2-weighted images and lack of restricted diffusion (34). These tumors need further imaging evaluation of the whole spine to exclude leptomeningeal involvement, although metastases are more frequent in the lung and bone (35).

Paratesticular tumors are isointense to the testicle on T1-weighted images and heterogeneously hyperintense to the testicle on T2-weighted images, with heterogeneous enhancement after contrast material administration (29,36).

Tumors arising in the genitourinary system have the same MRI features on T1- and T2-weighted images as other rhabdomyosarcomas.

Table 5: Differential Diagnosis of Soft-Tissue Sarcomas in Children

Sarcoma Type and Subtype	Location	Epidemiologic Features	Pathologic or Molecular Biology Features	Key Imaging Features	Treatment
Embryonal rhabdomyosarcoma					
Spindle cell	Head and neck	50% of all rhabdomyosarcomas 50% parameningeal, 20% nonparameningeal, 25% periorbital	MyoD1 Myogenin	Large mass in neck with internal necrosis	Chemotherapy + surgery ± RT
	Retroperitoneum, paratesticular	<10 y of age at presentation	MyoD1 Myogenin	High ADC due to necrosis and myxoid component	Chemotherapy + surgery
Botryoid	Bladder, prostate, vagina, biliary tree	<10 y of age at presentation	MyoD1 Myogenin	Large mass with lobules and necrosis	Chemotherapy + surgery ± RT
Alveolar rhabdomyosarcoma	Extremities, trunk	Presentation in infancy or adolescence	MyoD1 *PAX3-FOXO1* or *PAX7-FOXO1* fusion	Small foci of internal necrosis Bone involvement in 25%	Chemotherapy + surgery ± RT
MPNST	Extremities	Related to NF1 in 40%	S100 positivity in 50% of tumors	Intratumor necrosis Peritumor edema Peripheral enhancement	Surgery ± chemotherapy ± RT
Synovial sarcoma	Lower extremity around knee	Second most common soft-tissue sarcoma Less than 5% arise from synovium	Monophasic or biphasic Focal expression to epithelial markers	"Triple signal intensity" sign Calcification in 30% of patients 5% may mimic benign lesion	Chemotherapy + surgery
Extraosseous Ewing sarcoma	Lower extremity	20 mo to 30 y of age at presentation	Small round blue cells CD99 and FLI-1 positivity t(11;22)(q24;q12)	High-flow vascular channels with all sequences Microcystic appearance on T2-weighted images	Chemotherapy + surgery ± RT
Infantile fibrosarcoma	Extremities	Mean age of presentation 3 mo Present at birth in 40%	Spindle-shaped cells t(12;15)(p13;q25) ETV6-NTRK3 oncoprotein	Nonspecific Large mass with bone erosion Calcification in 35% of cases	Surgery ± chemotherapy
Epithelioid sarcoma	Hand, wrist	10–35 y of age at presentation	Large epithelioid or spindle cells Epithelial markers Loss of INI1 expression	Solid nodule surrounding tendon sheaths with avid enhancement	Surgery ± RT
Extrarenal rhabdoid tumor	Trunk, mediastinum	Presentation during 1st year of life	Rhabdoid cells Loss of INI1 expression	Large heterogeneous mass with central necrosis	Chemotherapy + surgery + RT

Note.—MPNST = malignant peripheral nerve sheath tumor, NF1 = neurofibromatosis type 1, RT = radiation therapy.

There is a variable degree of enhancement after intravenous contrast material administration depending on the size of the tumor, as internal vascularization decreases with tumor growth owing to internal necrosis (Fig 5) (37).

Botryoid rhabdomyosarcoma of the biliary tree may be difficult to distinguish from other hepatic masses—such as hepatoblastoma and undifferentiated embryonal sarcoma—owing to its large size at presentation (37) (Fig 6). The key imaging feature in this sarcoma is origin in and involvement of the biliary tree. At conventional MRI, these tumors are isointense to the liver on T1-weighted images and heterogeneously hyperintense to the liver on T2-weighted images, with central areas of necrosis that appear as heterogeneous areas of high T2 signal intensity with no enhancement after contrast material administration (30).

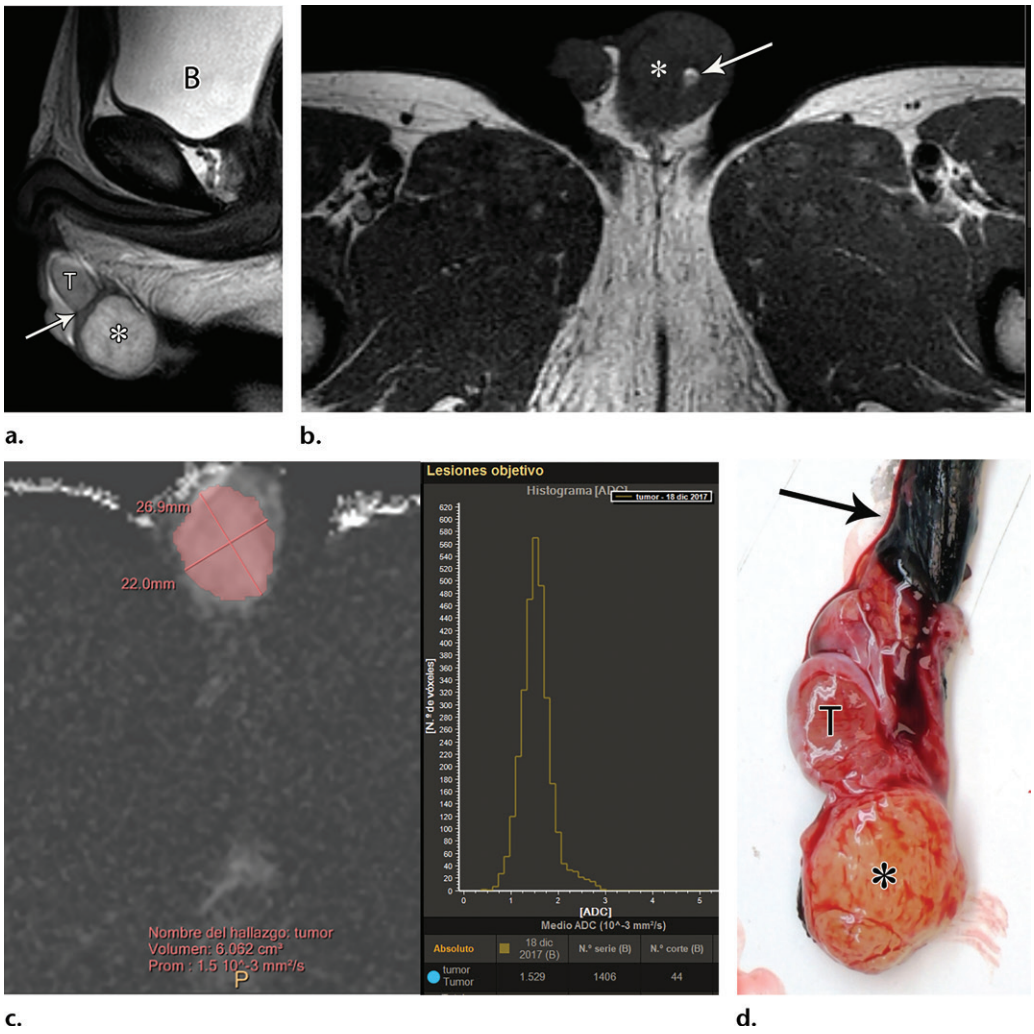

Figure 3. Paratesticular embryonal rhabdomyosarcoma involving the left hemiscrotum in a 4-year-old boy. **(a)** Sagittal T2-weighted image shows a heterogeneously hyperintense intrascrotal round lesion (*) with no clear plane of separation (arrow) from the adjacent testicle *(T)*. *B* = bladder. **(b)** Axial T1-weighted image shows that the mass (*) is predominantly isointense to muscle, although it contains small hyperintense foci (arrow), which may represent hemorrhage. **(c)** Left: Image from volumetric determination of ADC shows a tumor volume of 6 mL with ADC of 1.5 × 10^{-3} mm^2/sec. Right: The ADC histogram is high and sharp. **(d)** Photograph of the surgical specimen shows a yellowish tumor (*) with abundant myxoid component, which correlates with high ADC. The spermatic cord is dark (arrow) owing to postsurgical hemorrhage. *T* = testis.

Multiparametric MRI Findings.—Owing to its high cellularity, embryonal rhabdomyosarcoma usually shows restricted diffusion, which correlates with low ADC (34). Whole-lesion ADC histogram analysis along with DCE MRI assessment before and after treatment offer a quantitative interpretation of tumor response (19,22).

TICs performed in solid areas correlate with type III and IV curve profiles at DCE MRI, whereas curves performed in areas of hyperintensity on T2-weighted images show a type I curve profile, indicating necrosis or myxoid component (13,18,21,22). After surgery, residual tumor may exhibit type III and IV curve profiles, whereas granulation tissue and fibrosis show type II and V curve profiles.

At DWI, paratesticular tumor does not show restricted diffusion owing to its myxoid component, which correlates with the heterogeneous hyperintensity on T2-weighted images (13,18,34). Whole-lesion ADC histogram analysis of embryonal rhabdomyosarcoma does not usually demonstrate restriction as a consequence of internal necrosis and myxoid component.

Treatment.—Treatment of embryonal rhabdomyosarcoma depends on the subtype and anatomic location but is mainly based on a combination of chemotherapy drugs. Surgery and radiation therapy may be indicated on a case-by-case basis, depending on tumor location and stage (38). This plan has been proposed by the Children's Oncology Group (COG) in the

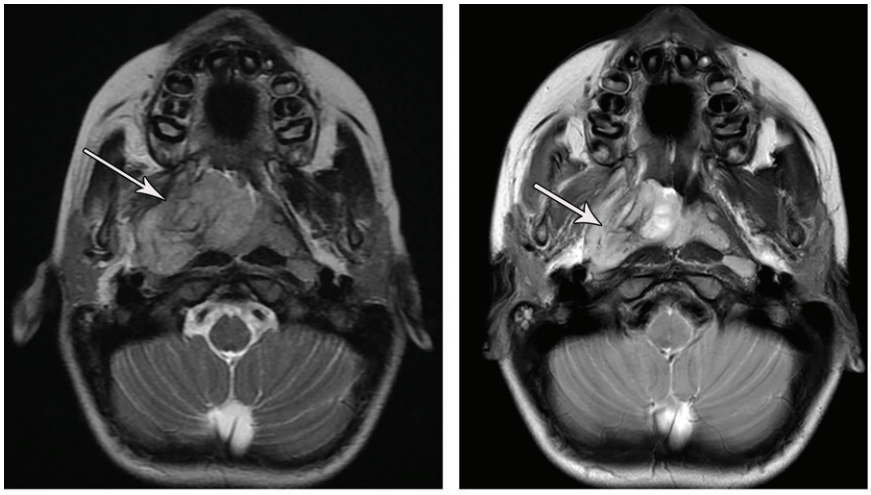

a. b.

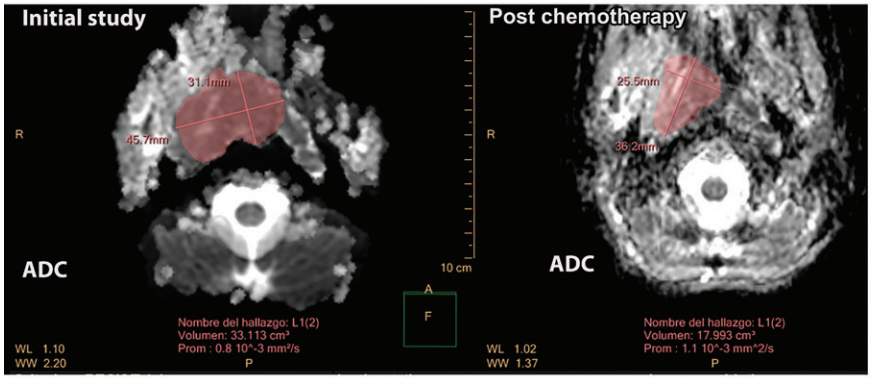

c.

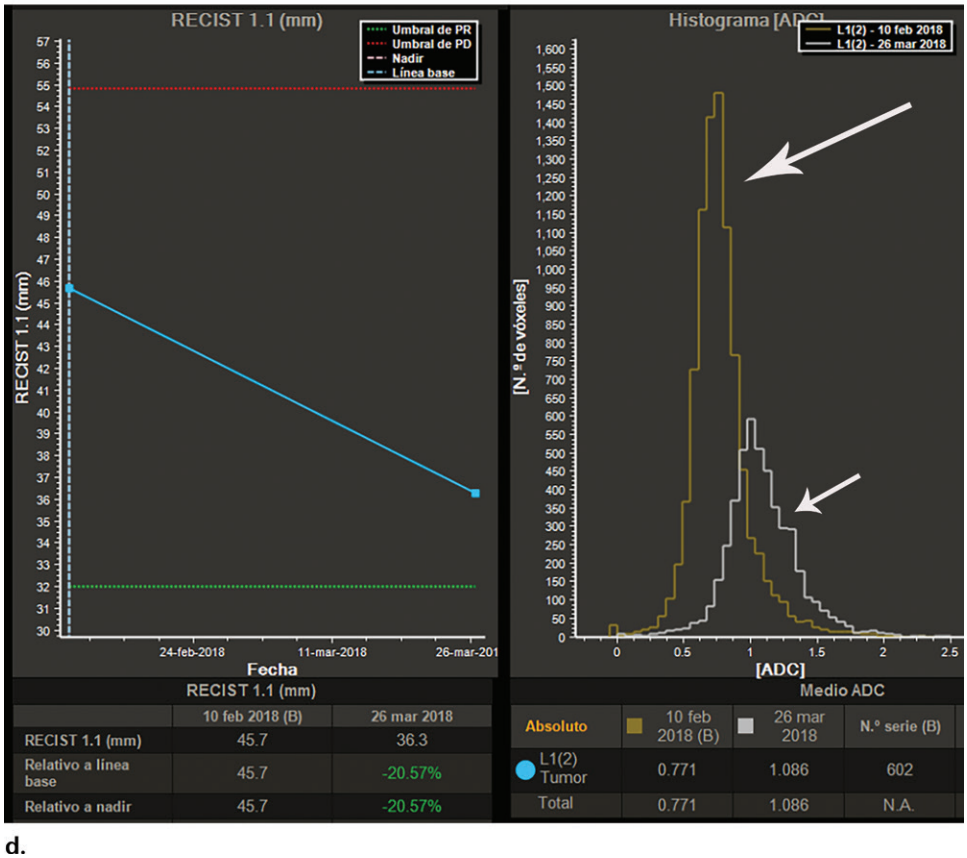

RECIST 1.1 (mm)	10 feb 2018 (B)	26 mar 2018
RECIST 1.1 (mm)	45.7	36.3
Relativo a línea base	45.7	-20.57%
Relativo a nadir	45.7	-20.57%

Absoluto	10 feb 2018 (B)	26 mar 2018	N.º serie (B)
L1(2) Tumor	0.771	1.086	602
Total	0.771	1.086	N.A.

d.

Figure 4. Embryonal rhabdomyosarcoma involving the parapharyngeal space in a 7-year-old boy. **(a)** Axial T2-weighted image shows a heterogeneously hyperintense lobulated mass (arrow) in the right parapharyngeal space. **(b)** Axial T2-weighted image 1 month after treatment shows decrease in size of the mass (arrow). **(c)** Images from volumetric determination of ADC show initial tumor volume of 33 mL (left) and volume after 1 month of treatment of 18 mL (right). **(d)** Graphs from volumetric determination of ADC before treatment show ADC of 0.77×10^{-3} mm^2/sec with a high and sharp ADC histogram (large arrow). The ADC after one cycle of chemotherapy was 1.09×10^{-3} mm^2/sec with a corresponding short and wide ADC histogram with rightward shift (small arrow).

Table 6: MRI Features of Soft-Tissue Sarcomas in Children

Sarcoma Type and Subtype	Location	MRI Appearance				
		T1W	T2W	T1W FS + CE	DWI Diffusion	DCE Curve Profiles
Embryonal rhabdomyosarcoma						
Spindle cell	Head and neck	Iso- to hyperintense to muscle	Heterogeneously hyperintense to muscle owing to necrosis or hemorrhage	Heterogeneous enhancement due to necrosis	Restricted in solid areas; no restriction in areas of necrosis or hemorrhage	Type III or IV in solid areas; type I in necrotic areas
	Retroperitoneum	Predominantly hypointense to muscle owing to necrosis	Heterogeneously hyperintense to muscle owing to necrosis or hemorrhage	Heterogeneous enhancement due to necrosis	Restricted in solid areas; no restriction in areas of necrosis or hemorrhage	Type III or IV in solid areas; type I in necrotic areas
	Paratesticular	Isointense to testicle	Heterogeneously hyperintense to testicle	Heterogeneous enhancement	No restriction owing to necrosis or myxoid component	Type III or IV
Botryoid	Bladder, prostate, vagina, biliary tree	Iso- to hyperintense to muscle	Heterogeneously hyperintense to muscle owing to necrosis or hemorrhage	Internal vascularization decreases with tumor growth owing to internal necrosis	Restricted in solid areas; no restriction in areas of necrosis or hemorrhage	Type III or IV in solid areas; type I in necrotic areas
Alveolar rhabdomyosarcoma	Extremities, trunk	Iso- to hyperintense to muscle Erosions	Heterogeneously hyperintense to muscle Fascial involvement	Heterogeneous enhancement	Restricted	Type III or IV
MPNST	Extremities	Isointense to muscle	Perilesion edema-like zone and intratumor necrosis	Peripheral enhancement pattern	Restricted in solid areas; no restriction in areas of necrosis or hemorrhage	Type III or IV in solid areas; type I in necrotic areas
Synovial sarcoma	Lower extremity around knee	Heterogeneous internal signal intensity	Heterogeneous internal signal intensity "Triple signal intensity" sign	Heterogeneous enhancement due to internal necrosis, hemorrhage, calcification, and cystic areas	Restricted in solid areas; no restriction in areas of necrosis or hemorrhage	Type III or IV in solid areas; type I in necrotic areas
Extraosseous Ewing sarcoma	Lower extremity	Hypo- to isointense	High signal intensity Microcystic appearance	Heterogeneous enhancement with internal foci of necrosis	Restricted	Type III or IV
Infantile fibrosarcoma	Extremities	Hypo- to isointense Cortical thickening, bending deformities, and erosions	Hyperintense	Heterogeneous enhancement	Restricted owing to high cellularity	Type III or IV
Epithelioid sarcoma	Hand, wrist	Homogeneously isointense	Homogeneously hyperintense	Homogeneous enhancement	Restricted owing to high cellularity	Type III or IV
Extrarenal rhabdoid tumor	Trunk, mediastinum	Hypo- to isointense	Heterogeneously hyperintense	Heterogeneous and peripheral enhancement due to necrosis	Restricted in solid areas; no restriction in necrotic areas	Type III or IV in solid areas; type I in necrotic areas

Note.—CE = contrast-enhanced, FS = fat-suppressed, MPNST = malignant peripheral nerve sheath tumor, T1W = T1-weighted, T2W = T2-weighted.

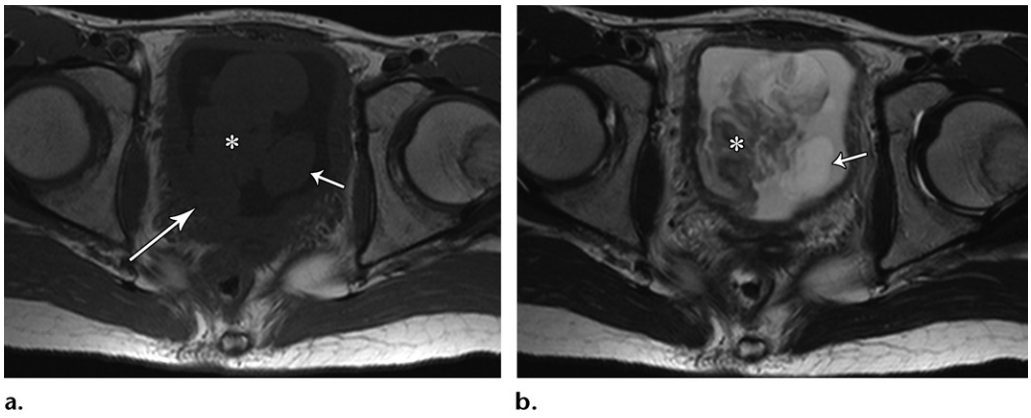

a. b.

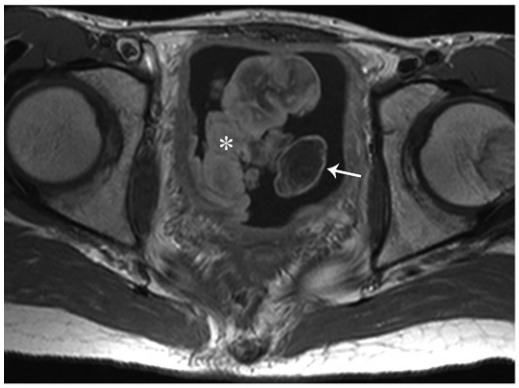

c.

Figure 5. Embryonal rhabdomyosarcoma (botryoid variant) of the bladder in a 5-year-old girl. **(a)** Axial T1-weighted image shows a multilobulated mass (arrows) arising from the right posterolateral wall of the bladder and protruding into the bladder lumen. The mass (*) is isointense to muscle. **(b)** Axial T2-weighted image shows areas of heterogeneous hypointensity (*) and areas of high signal intensity (arrow) in the lesion, which may represent solid component and necrosis, respectively. **(c)** Axial contrast-enhanced fat-suppressed T1-weighted image shows heterogeneous enhancement of the mass (*) in association with areas that lack enhancement (arrow), which are suggestive of necrosis.

United States and the more recently founded European Pediatric Soft Tissue Sarcoma Study Group (EpSSG) in Europe (5,38). The reported 5-year survival rate exceeds 70% for patients with localized rhabdomyosarcoma (38).

Alveolar Rhabdomyosarcoma

Epidemiologic Features.—Alveolar rhabdomyosarcoma represents 15%–20% of all rhabdomyosarcomas and is more common in older children and young adults, typically between 10 and 25 years of age (24).

Clinical Features.—Alveolar rhabdomyosarcoma manifests as a painless mass of indolent growth, as it usually arises in the deep soft tissues of the extremities and trunk (23,32).

Histopathologic Findings.—Alveolar rhabdomyosarcoma is a highly cellular tumor with fibrous stroma and fibrovascular septa that tends to peripheral discohesion with an alveoli-like appearance. The expression of myogenin is typically stronger and more diffuse than in embryonal rhabdomyosarcoma (39). Alveolar rhabdomyosarcoma has consistent translocations, resulting in fusion of a transcription factor with the genes *PAX3* or *PAX7*.

There is a well-established algorithm protocol for histopathologic diagnosis of alveolar rhabdomyosarcoma, which includes a multidisciplinary team of radiologists, pathologists, and molecular biologists (Fig 7) (40).

Conventional MRI Findings.—Findings are similar to those in other soft-tissue sarcomas, with the lesion being iso- to hyperintense to muscle on T1-weighted images and heterogeneously hyperintense to muscle on T2-weighted images (Fig 8) (41,42). Involvement of adjacent bone with erosions or subperiosteal new bone formation is found in approximately 25% of patients (6,42). Alveolar rhabdomyosarcoma typically shows muscle and fascial involvement.

Multiparametric MRI Findings.—As with other variants of rhabdomyosarcoma, alveolar rhabdomyosarcoma shows restricted diffusion, which correlates with low ADC. DCE MRI curves performed in solid areas correlate with type III or IV profiles, whereas curves performed in areas of necrosis show a type I profile. Some of these tumors may be unresectable, depending on the location, and use of DCE MRI and TICs is valuable (19,21). As with other tumors, residual tumor typically shows type III or IV curve profiles, whereas fibrosis may show a type V profile (22).

Treatment.—The survival of children with nonmetastatic rhabdomyosarcoma has significantly improved in the past few years owing to a multimodality therapy approach, which includes

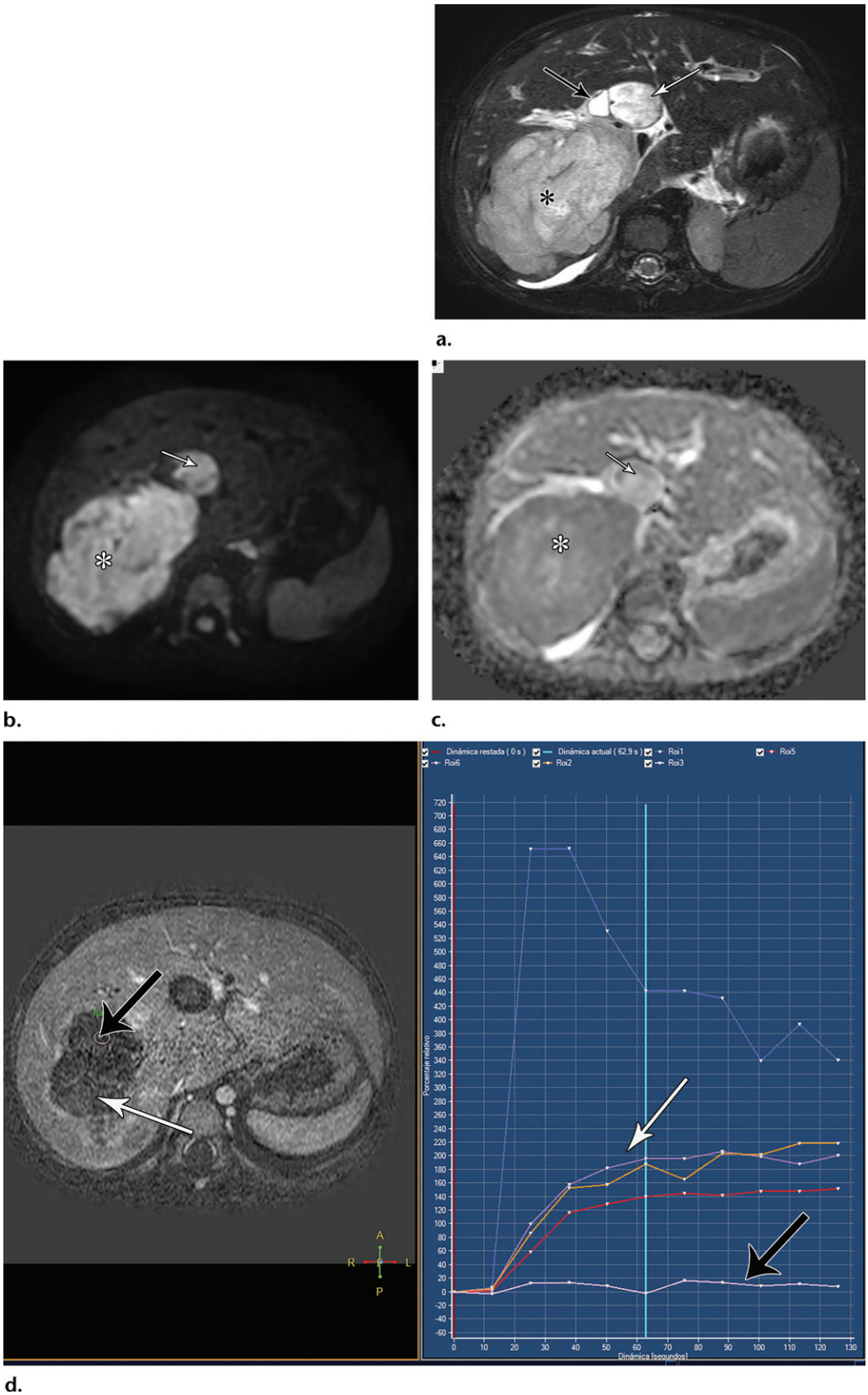

Figure 6. Embryonal rhabdomyosarcoma (botryoid variant) of the liver in a 3-year-old boy. **(a)** Axial fat-suppressed T2-weighted image shows a heterogeneously hyperintense liver mass (*) with lobulated margins. The lesion involves and expands the common bile duct (CBD) (white arrow) in association with proximal dilatation of the biliary tree (black arrow). **(b, c)** Axial diffusion-weighted image **(b)** and ADC image **(c)** show restricted diffusion of the mass (*) and of the tumoral component in the CBD (arrow). **(d)** Left: DCE image shows heterogeneous enhancement of the mass (white arrow). The mass also contains areas of necrosis (black arrow). Right: The heterogeneous enhancement correlates with a type III or IV TIC profile (white arrow). The areas of necrosis correlate with a type I curve profile (black arrow). Blue curve = reference standard of arterial uptake.

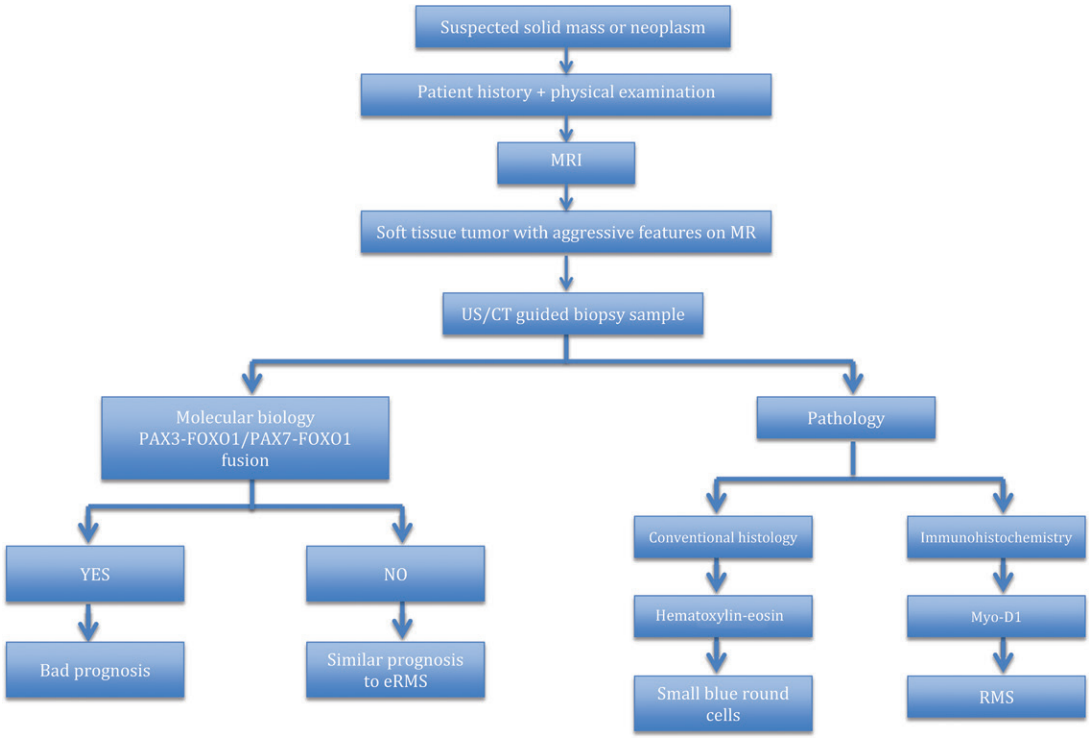

Figure 7. Algorithm for histopathologic diagnosis of alveolar rhabdomyosarcoma *(RMS)*. *eRMS* = embryonal rhabdomyosarcoma.

chemotherapy along with surgery and in some cases radiation therapy (43,44). The reported 5-year survival rate exceeds 70% for patients with localized rhabdomyosarcoma (45).

The alveolar type has the worst prognosis among all rhabdomyosarcomas. Up to 15% of patients with alveolar rhabdomyosarcoma have metastasis at presentation (6,41,42), and up to 79% develop metastasis during the disease course, most frequently in the bone, lung, or bone marrow (41,45). These metastases have the same imaging features as the original tumor.

The differential diagnosis of rhabdomyosarcoma is broad and varies depending on tumor type, location, and size and the age at presentation. In the head and neck, lymphoma and leukemia as well as nasopharyngeal carcinoma should be considered (6,41). In the retroperitoneum, the differential diagnosis includes germ cell tumors. In the extremities and trunk, the differential diagnosis includes other soft-tissue sarcomas, such as synovial sarcoma and extraosseus Ewing sarcoma (41).

Malignant Peripheral Nerve Sheath Tumor

Epidemiologic Features.—MPNST is a rare malignant tumor, accounting for approximately 2% of all soft-tissue sarcomas (2,6,41,46). It arises from a peripheral nerve and may manifest in the following scenarios: de novo in approximately 50% of cases, related to NF1 in up to 40% of cases (46,47), and secondary to radiation therapy in less than 10% of cases (47). Patients with NF1 have an estimated 13% lifetime risk of developing MPNST, mainly arising in a preexisting plexiform neurofibroma (46), making the diagnosis of MPNST relatively easy to suspect in these patients.

MPNST is highly aggressive, with metastasis in up to 25% of patients at diagnosis and a tendency to recur locally (46).

Clinical Features.—As with other soft-tissue sarcomas, the clinical features depend to a large extent on the location of the tumor (2,6,41,42).

Histopathologic Findings.—MPNST is a high-grade tumor, composed of spindle cells tightly packed in a fascicular pattern (48). In NF1, most MPNSTs arise in neurofibromas. In these cases, they can show areas of transition from neurofibroma, with increased cellularity but without malignant features of MPNST. Distinction of atypical neurofibroma from MPNST can be difficult, especially in small biopsy samples. Tumor cells in MPNST show focal positivity for S100 in 50% of cases (49). Patients with NF1 carry germline alterations in the *NF1* gene (17q11.2), which encodes the tumor suppressor protein neurofibromin (48).

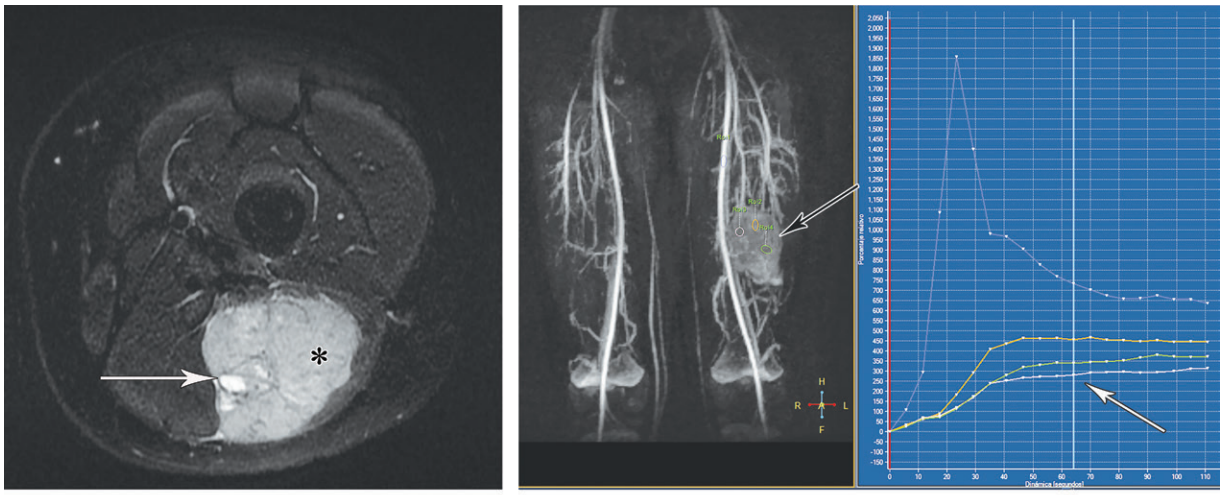

a. b.

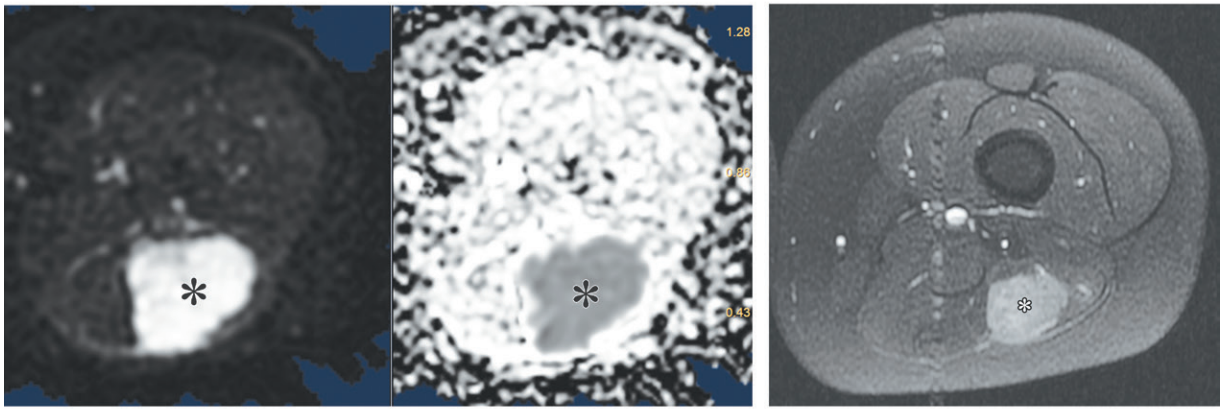

c. d.

e.

Figure 8. Alveolar rhabdomyosarcoma in an 11-year-old boy with a left thigh mass. **(a)** Axial fat-suppressed T2-weighted image shows a lobulated heterogeneously hyperintense lesion (*) with a peripheral cystic or necrotic component (arrow) involving the biceps femoris muscle. **(b)** DCE image shows diffuse early enhancement of the tumor (black arrow). This finding correlates with a type III or IV TIC profile (white arrow). Blue curve = reference standard of arterial uptake. **(c)** Axial diffusion-weighted image and ADC image show restricted diffusion in the mass (*). **(d)** Axial contrast-enhanced fat-suppressed T1-weighted image after chemotherapy shows significant shrinkage of the tumor (*), with persistence of heterogeneous enhancement. **(e)** Graphs from volumetric determination of ADC show ADC of 0.78 × 10^{-3} mm^2/sec with a high and sharp ADC histogram before treatment (white arrow). ADC after 2 months of treatment was 1.06 × 10^{-3} mm^2/sec with a short and wide ADC histogram with rightward shift (black arrow). There was 50% reduction of tumor volume in the interval.

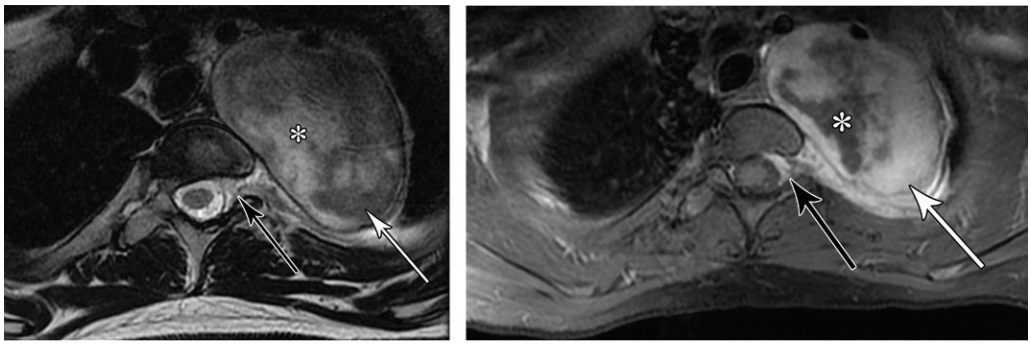

a. b.

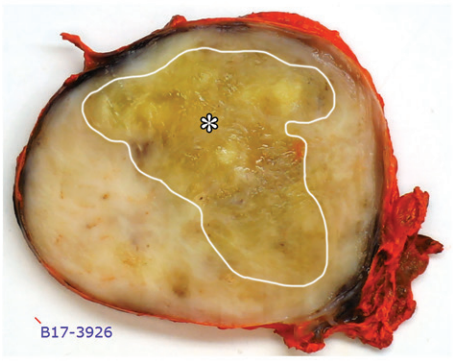

c.

Figure 9. MPNST in a 14-year-old boy with NF1. **(a)** Axial T2-weighted image shows a well-defined mass in the left mediastinum, which contains hypointense areas (white arrow) as well as hyperintense areas (*), the latter likely representing necrosis. Note the involvement of the adjacent neural foramen with extension of the mass into the spinal canal (black arrow). **(b)** Axial contrast-enhanced fat-suppressed T1-weighted image shows intense peripheral enhancement of the lesion (white arrow), with internal hypointense areas suggestive of necrosis (*). Black arrow = extension of the mass into the spinal canal. **(c)** Photograph of the surgical specimen shows an internal yellowish area suggestive of necrosis (*), which correlates with the areas described at MRI.

Conventional MRI Findings.—MPNST usually manifests as a large mass with ill-defined margins and intratumor lobules. It is isointense to muscle on T1-weighted images and heterogeneously hyperintense on T2-weighted images, typically with heterogeneous enhancement (Fig 9) (50,51). Some of the MRI features that may help differentiate this tumor from plexiform neurofibroma include its large size, disproportionate growth at follow-up examinations, peripheral enhancement pattern, perilesion edema-like zone, and intratumor necrosis (50–52).

Whole-body MRI is potentially useful to follow up patients with NF1 and to detect malignant transformation (53). If there is suspicion of MPNST, further evaluation of the region of concern with dedicated MRI is indicated to better characterize the tumor.

Multiparametric MRI Findings.—At DWI, MPNST typically shows diffusion restriction in solid areas, which correlates with type III and IV curve profiles at DCE MRI, whereas intratumor necrosis does not show diffusion restriction and exhibits a type I curve profile (4,12,21). As these tumors tend to recur locally, DCE MRI is the modality of choice for detecting recurrence by showing the same curve profile as the original tumor.

Treatment.—Biopsy is required for MPNST to ensure optimal surgical planning. The main goal of treatment is curative surgery with the objective of achieving wide surgical margins (54). Patients with unresectable tumors or excised tumors with positive margins undergo chemotherapy with a combination of doxorubicin and ifosfamide and radiation therapy. Despite this multimodal treatment, the prognosis for MPNST is poor, with a 5-year survival rate of 23%–69% (54). There is a 50% rate of local recurrence in the first 2 years after treatment (54).

Synovial Sarcoma

Epidemiologic Features.—Synovial sarcoma is the second most common soft-tissue sarcoma in children after rhabdomyosarcoma, affecting girls in 50%–70% of cases (55,56). The term *synovial* is misleading, as the tumor does not arise from synovium; in fact, less than 5% of these tumors arise in a joint or bursa (57,58). Up to 90% of synovial sarcomas involve the deep soft tissues of the extremities, usually around the knee and adjacent to joints or tendon sheaths (56).

Clinical Features.—Synovial sarcoma manifests as a slow-growing painless mass usually involving the lower extremity around the knee (55).

Histopathologic Findings.—There are two major subtypes: biphasic and monophasic spindle cell. The biphasic subtype has a combination of epithelial and spindle cells. More than 90% of

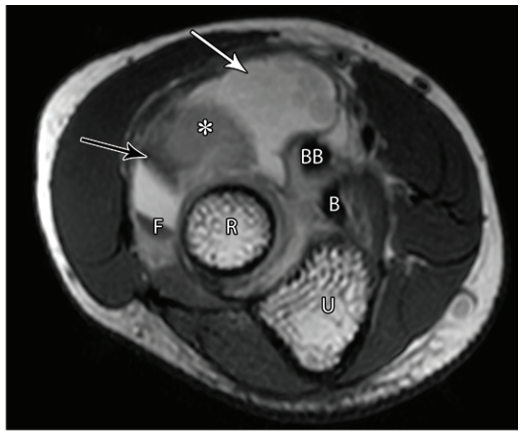

a.

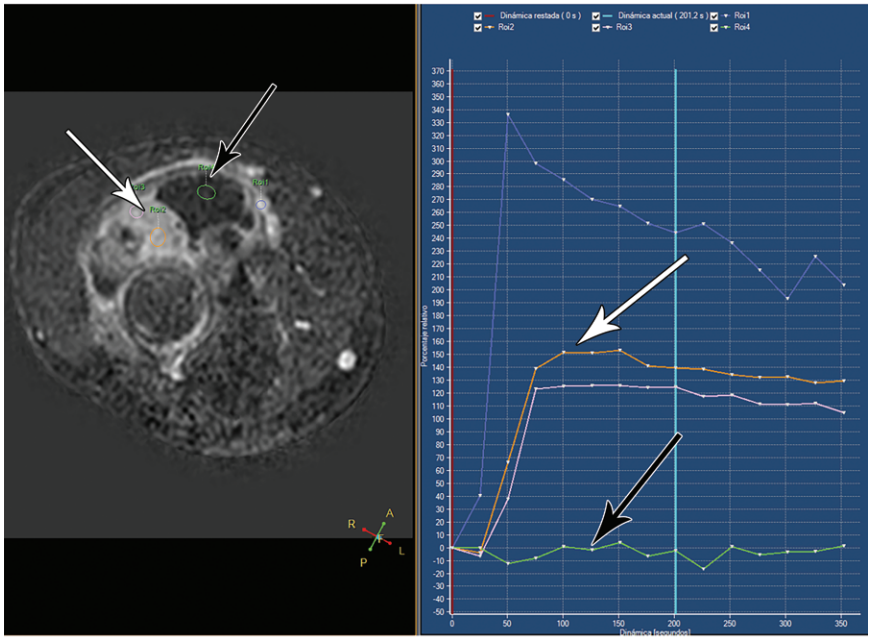

b.

Figure 10. Synovial sarcoma of the left elbow in a 12-year-old girl. **(a)** Axial T2-weighted image shows a multilobulated mass involving the supinator muscle with fluid levels *(F)*. The mass shows the "triple signal intensity" sign: cystic or necrotic component (white arrow), solid component (*), and fibrosis or calcification (black arrow). *B* = brachialis tendon, *BB* = biceps brachii, *R* = radius, *U* = ulna. **(b)** Left: DCE image shows intense enhancement of the tumor (white arrow). The lesion also contains areas of necrosis (black arrow). Right: The areas of intense enhancement correlate with a type III or IV TIC profile (white arrow). The areas of necrosis correlate with a type I curve profile (black arrow). Blue curve = reference standard of arterial uptake.

synovial sarcomas, including all histologic subtypes, show focal expression of epithelial markers (59). Synovial sarcoma is characterized by the translocation t(X;18)(p11;q11), which is found exclusively in this tumor (59).

Conventional MRI Findings.—Synovial sarcoma is often a multilobulated mass with heterogeneous internal signal intensity on T1- and T2-weighted images. It shows inhomogeneous enhancement caused by internal necrosis, hemorrhage, calcification, and cystic areas (57,58).

Up to 5% of the tumors may manifest at MRI as benign-appearing masses, especially when they are small, well-defined, and encapsulated, mimicking the appearance of popliteal cysts, hematomas, or ganglion cysts (58). Use of intravenous contrast material may be useful in these cases by showing enhancement of the solid component of the tumor.

At MRI, triple signal intensity in a soft-tissue mass has been described as a highly suggestive sign of synovial sarcoma (60). This is seen on non–fat-suppressed T2-weighted images as hyperintense, isointense, and hypointense intratumor areas as compared with fat, which reflect necrosis or cystic degeneration (hyperintensity), solid component or cellularity (isointensity), and calcification or fibrotic bands (hypointensity) (Fig 10) (60).

Calcification is not rare, described in about 30% of cases. Fluid levels are caused by internal necrosis and hemorrhage and are more frequently seen in larger tumors (60).

Multiparametric MRI Findings.—DCE MRI shows early enhancement of solid areas, correlating with a type III or IV curve profile (61). Necrotic or cystic degeneration in the tumor exhibits a type I curve profile. If a small, well-defined, benign-appearing mass, located adjacent to joints,

tendon sheaths, or bursae, has early enhancement at DCE MRI, synovial sarcoma needs to be included in the differential diagnosis (58,60). Use of DWI, DCE MRI, and TICs in follow-up examinations is highly recommended, as these tumors have a high rate of local recurrence. Tumor recurrence behaves like the original tumor, showing restricted diffusion on ADC maps and a type III or IV curve profile at DCE MRI (22).

The differential diagnosis may include other soft-tissue sarcomas such as rhabdomyosarcoma and extraosseous Ewing sarcoma (6,41,42).

Treatment.—Biopsy is required for appropriate treatment planning. Chemotherapy and surgery are the mainstays of treatment. If clear margins cannot be achieved with surgery, radiation therapy is indicated (62). Up to 25% of patients have metastasis at diagnosis, and 50% present with local recurrence in the first 2 years after diagnosis (56,62).

Ewing Sarcoma Family Tumors: Extraosseous Ewing Sarcoma

Epidemiologic Features.—Ewing sarcoma family tumors comprise Ewing sarcoma of bone, primitive neuroectodermal tumor (PNET) or peripheral neuroepithelioma, extraosseous Ewing sarcoma, and Askin tumor (also known as PNET of the chest wall) (63).

All of these tumors arise from the same stem cell. They have equal gender distribution, and the age at presentation ranges from 20 months to 30 years, with an average age of 20 years. The mean age is higher than that in Ewing sarcoma of bone (64).

The most frequent sites of involvement include the lower extremity, paravertebral region, head and neck, and pelvis (63). Tumors located adjacent to bone may cause cortical erosion and subperiosteal new bone formation.

Clinical Features.—These tumors usually manifest as a large, solitary, superficial or deep soft-tissue mass measuring 5–10 cm at initial presentation. As a result of their rapid growth, they tend to be locally aggressive and may involve surrounding structures. Tumors arising in the paravertebral region or spinal canal may manifest as back pain, scoliosis, extremity weakness or paresthesia, or symptoms of bladder or bowel dysfunction (63).

Histopathologic Findings.—Extraosseous Ewing sarcoma is a small blue round cell tumor that displays variable neuroectodermal differentiation (64). Combination of CD99 and FLI-1 is the method of choice for diagnosis of this tumor (65), because Ewing sarcoma expresses characteristically diffuse and membranous CD99 positivity and strong nuclear staining for FLI-1. Nearly 85% of Ewing sarcomas demonstrate a chromosomal translocation—t(11;22)(q24;q12)—that fuses *EWSR1* to *FLI1* (65).

Conventional MRI Findings.—Extraosseous Ewing sarcoma usually manifests as a large well-defined soft-tissue mass, with low to intermediate signal intensity on T1-weighted images and high signal intensity on T2-weighted images (64). It typically has a microcystic appearance on T2-weighted images, resembling Ewing sarcoma of bone (Fig 11) (64). These tumors frequently contain areas of hemorrhage, which may appear hypo-, iso-, or hyperintense, depending on their time of evolution. Fluid levels due to internal hemorrhage may also be present, as well as calcifications, which are present in up to 25% of patients and are seen as small hypointense foci with all sequences (41,42,64).

High-flow vascular channels feeding the tumor have been additionally described at MRI. This is not a specific finding for extraskeletal Ewing sarcoma and can be seen in other soft-tissue sarcomas such as rhabdomyosarcoma, synovial sarcoma, and even high-flow vascular lesions, but its presence in the appropriate clinical setting should alert one to the diagnosis of Ewing sarcoma (42,64).

After administration of contrast material, these tumors often exhibit heterogeneous enhancement with internal foci of necrosis that do not enhance (64).

Multiparametric MRI Findings.—DWI shows restriction owing to the tumor's high grade of cellularity. Obtaining ADC histograms is a valuable tool for assessing tumor response, together with DCE MRI, which demonstrates a type III or IV curve profile. Residual tumor or local recurrence shows the same DCE MRI features as the original tumor, as well as the same TICs (22).

Treatment.—Standard treatment is based on a combination of neoadjuvant chemotherapy and surgery. If wide margins cannot be achieved with surgery, radiation therapy is indicated. Recurrence occurs in 30% of cases. Specific predictors for better survival are younger age and complete resection (65).

Infantile Fibrosarcoma

Epidemiologic Features.—Fibrosarcoma is an exceedingly rare soft-tissue sarcoma that can be classified into two categories: infantile (or congenital) type and adult type. The infantile type has a more favorable clinical course and prognosis than the adult type (66,67).

Figure 11. Extraosseous Ewing sarcoma of the right thigh in a 9-year-old girl. **(a)** Coronal T1-weighted image shows an ovoid slightly hyperintense mass (*) involving the vastus lateralis of the right quadriceps femoris muscle. Note the tortuous high-flow feeding vessels (arrow), a well-recognized finding of extraosseous Ewing sarcoma. **(b)** Coronal short τ inversion-recovery (STIR) image shows a heterogeneously hyperintense intramuscular mass (*) associated with hypointense serpentine high-flow feeding vessels (arrow). **(c)** Left: DCE image shows intense enhancement of the tumor (arrow). Right: This finding correlates with a type III or IV TIC profile (arrow). Blue curve = reference standard of arterial uptake. **(d)** Photograph of the surgical specimen shows a heterogeneous solid tumor (*) with tiny foci of internal hemorrhage (arrow).

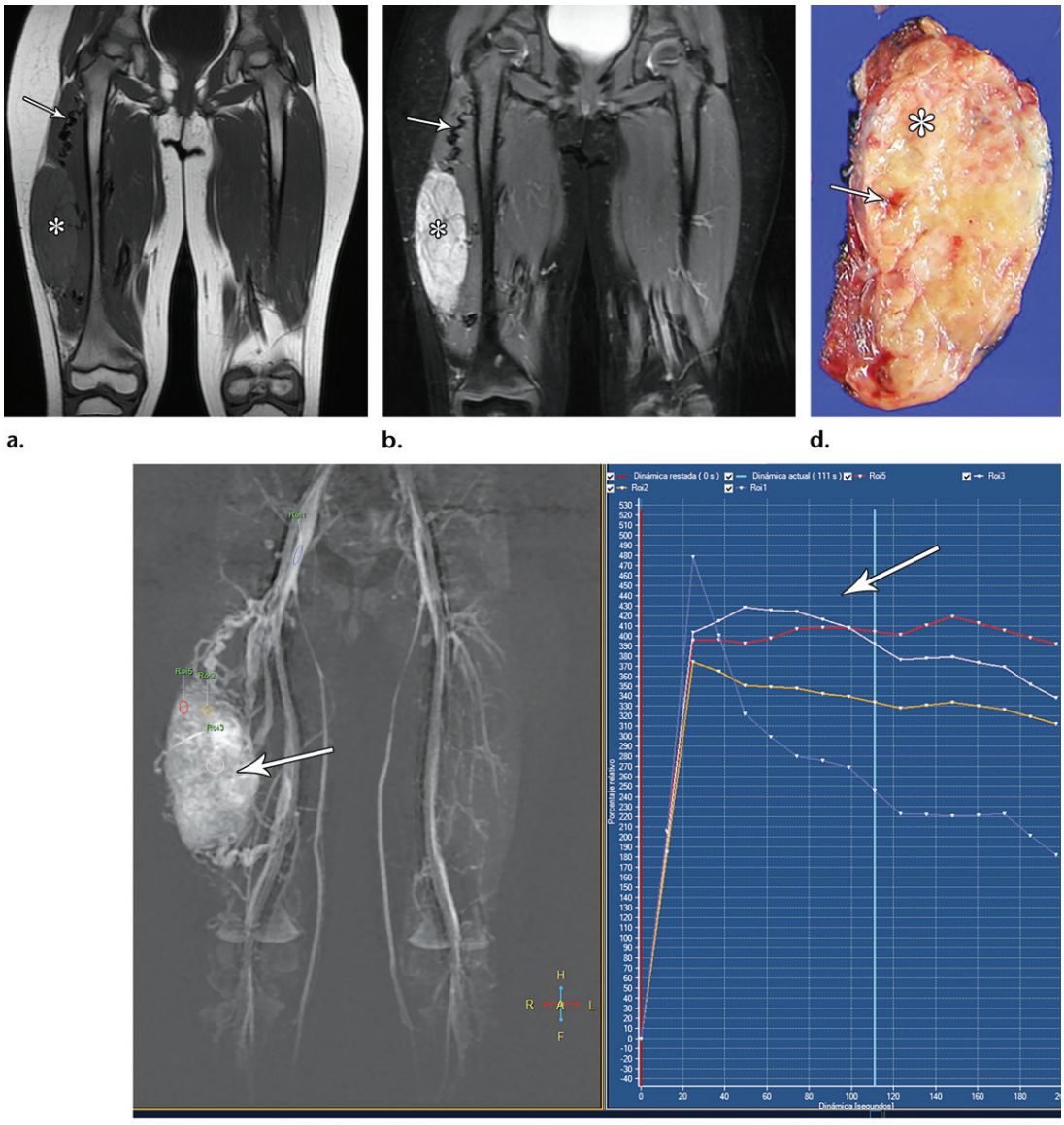

As implied by its name, infantile fibrosarcoma is predominantly seen in children, accounting for approximately 5%–10% of all pediatric sarcomas in the first 5 years of life. The mean age of presentation is 3 months, and approximately 40% are present at birth (68). Boys are more frequently affected than girls (66).

The extremities are the main site of involvement, and such tumors have a better prognosis and low rate of recurrence compared with tumors arising in the trunk, head and neck, retroperitoneum, mesentery, or orbit, which usually have a high tendency to metastasize (69).

Clinical Features.—Infantile fibrosarcoma often manifests as a painless mass that ranges from small to massive with rapidly progressive growth. Clinically, the skin color overlying the lesion may resemble the discoloration seen with hemangiomas (66,67).

Histopathologic Findings.—Infantile fibrosarcoma shows a morphologic spectrum from highly cellular tumor to less cellular areas. It is associated with a recurrent translocation—t(12;15)(p13;q25)—that fuses *ETV6* to *NTRK3*, generating fusion transcripts encoding the ETV6-

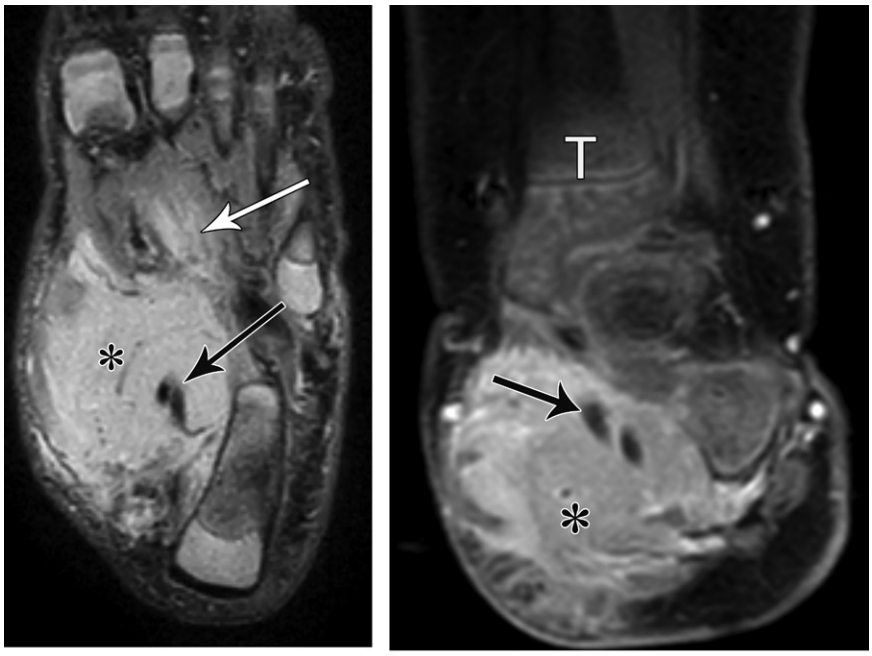

a. b.

Figure 12. Congenital fibrosarcoma of the left foot in a 3-month-old girl. **(a)** Long-axis fat-suppressed T2-weighted image shows an irregular mass (*) with ill-defined margins involving the medial aspect of the foot, with invasion of the plantar muscles (white arrow). The mass has relatively homogeneous high signal intensity. The tibialis posterior and flexor hallucis longus tendons (black arrow) are encased by the mass. **(b)** Short-axis contrast-enhanced fat-suppressed T1-weighted image shows avid enhancement of the mass (*). Arrow = encased tendons, *T* = tibia.

NTRK3 oncoprotein, which is a potential diagnostic marker for infantile fibrosarcoma (70).

Conventional MRI Findings.—Infantile fibrosarcoma is hypo- to isointense on T1-weighted images and hyperintense on T2-weighted images, with heterogeneous enhancement after administration of contrast material (Fig 12) (69). The tumor may involve the underlying bone and show cortical thickening, bending deformities, and erosions (69,71). Calcifications may be present in 35% of cases, appearing as hypointense foci with all sequences (69).

Multiparametric MRI Findings.—At DWI, infantile fibrosarcoma usually shows diffusion restriction owing to its high cellularity. DCE MRI shows type III or IV curve profiles. In areas where the tumor cannot be completely excised, DWI and DCE MRI play an important role in assessing for tumor response and residual disease.

Treatment.—If the tumor is confined to a specific region of the body, the mainstay therapy is surgical resection with clear margins. However, when the neurovascular bundle is involved or the tumor affects the entire extremity, amputation is indicated.

Compared with other soft-tissue sarcomas, infantile fibrosarcoma has a better prognosis, with a reported overall survival rate of 90% at 5 years (69,71). Although local recurrence is relatively common, with a 50% rate in the first 2 years, metastatic disease is rare and the long-term survival rate is high. The location and extent of disease at diagnosis are the most relevant prognostic factors.

Epithelioid Sarcoma

Epidemiologic Features.—Epithelioid sarcoma is a rare entity. However, it is the most common soft-tissue sarcoma of the hand and wrist in adolescents and young adults up to 35 years of age. Males are more frequently affected than females. It usually arises from the tendon sheaths of the fingers and hands but may also arise in other sites, including the musculature (72).

Clinical Features.—Epithelioid sarcoma manifests as a slow-growing painless mass, usually involving the fingers. When small, it may be mistaken for giant cell tumor of the tendon sheath or fibroma of the tendon sheath. Larger lesions, frequently arising from the tendons and fascial structures, may be misdiagnosed as synovial sarcoma or fibrosarcoma (41,42).

Histopathologic Findings.—There are two types of epithelioid sarcoma: the conventional or classic type, which affects mainly the hands and feet, and the proximal type, which affects mainly the deep truncal soft tissues, more often in older people (73).

Tumor cells exhibit immunoreactivity for epithelial markers, especially epithelial membrane antigen (EMA). Loss of INI1 expression is characteristic (74). Epithelioid sarcoma has alterations in the *SMARCB1* gene at 22q11, which have been implicated in the pathogenesis of most of these tumors.

Conventional MRI Findings.—Tumors are homogeneously isointense to muscle on T1-weighted

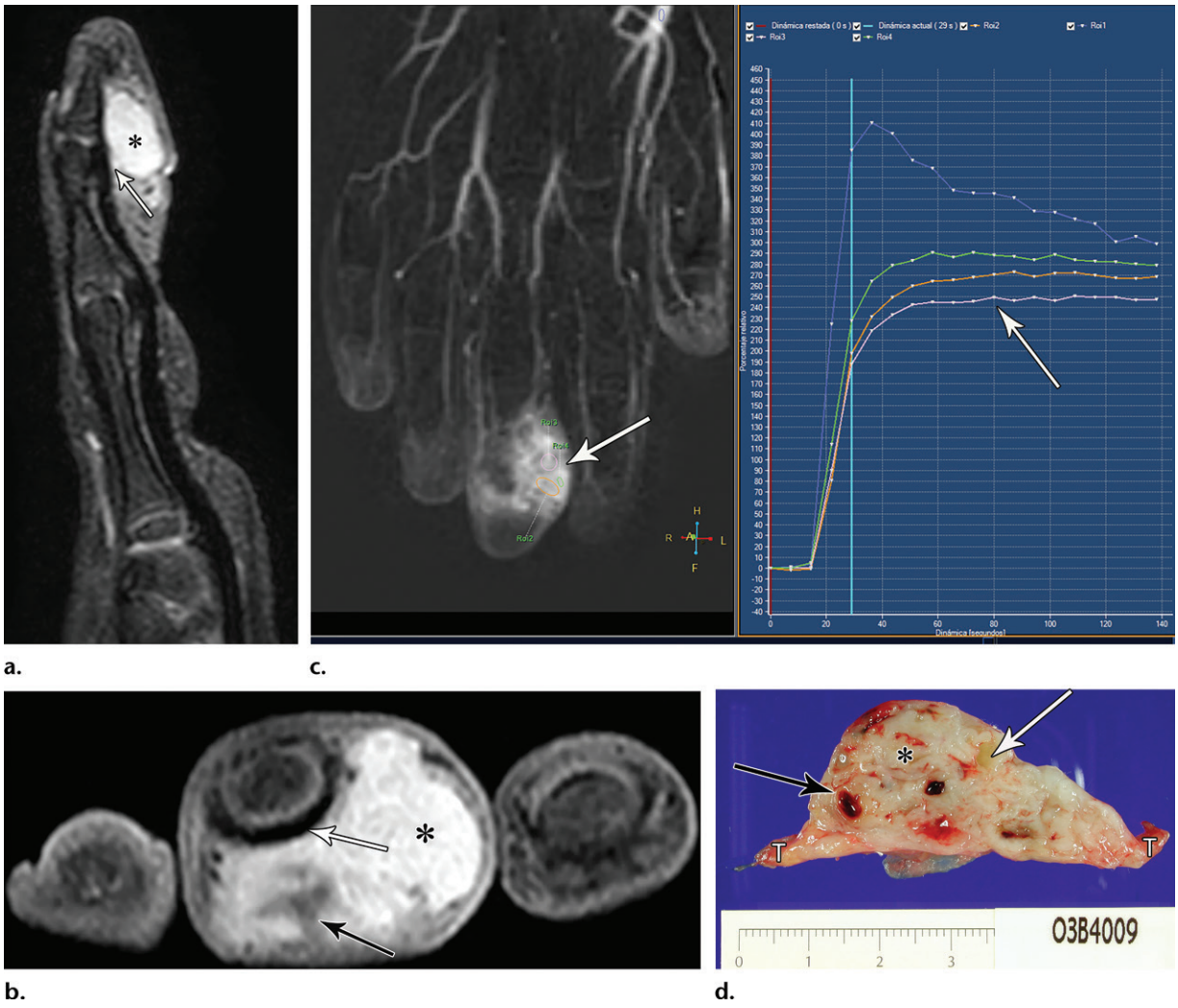

Figure 13. Epithelioid sarcoma involving the subcutaneous soft tissues of the distal second right finger in a 10-year-old boy. **(a)** Sagittal fat-suppressed T2-weighted image shows a well-defined lobulated mass of homogeneous high signal intensity (*). There is absence of a cleavage plane between the flexor tendon (arrow) and the mass. **(b)** Axial contrast-enhanced fat-suppressed T1-weighted image shows diffuse intense enhancement of the mass (*), with small internal areas of hypointensity (black arrow) suggestive of necrosis. Note the close relation of the mass to the flexor tendon (white arrow). **(c)** Left: DCE image shows intense enhancement of the mass (arrow). Right: This finding correlates with a type III or IV TIC profile (arrow). Blue curve = reference standard of arterial uptake. **(d)** Photograph of the surgical specimen shows a heterogeneous solid tumor (*) with tiny areas of necrosis (white arrow) and hemorrhage (black arrow). *T* = tendon.

images and homogeneously hyperintense to muscle on T2-weighted images, with homogeneous enhancement after administration of contrast material (72) (Fig 13).

Multiparametric MRI Findings.—Epithelioid sarcomas are highly cellular tumors and usually show restricted diffusion. DCE MRI shows early intense enhancement, correlating with a type III or IV curve profile, as with other soft-tissue sarcomas. As these tumors have a high rate of recurrence, use of DWI and DCE MRI after tumor excision is mandatory to evaluate for recurrence.

Treatment.—Surgery is the mainstay of treatment, followed by radiation therapy if margins are affected. Despite the presence of wide surgical margins, epithelioid sarcoma has a high rate of local recurrence with a tendency to metastasize to regional lymph nodes (43).

Extrarenal Malignant Rhabdoid Tumor

Epidemiologic Features.—Malignant rhabdoid tumor is an aggressive pediatric sarcoma that was initially described in the kidneys by Beckwith and Palmer (75) in 1978 as an aggressive rhabdomyosarcomatous variant of Wilms tumor. Rhabdoid tumor can be divided into renal and extrarenal types according to its site of origin.

The extrarenal type of rhabdoid tumor is an exceedingly rare and highly malignant tumor with median age at presentation of 11 months, but it

Figure 14. Extrarenal rhabdoid tumor in a newborn. **(a)** Sagittal T2-weighted image shows a large mass involving the subcutaneous fat at the posterior aspect of the neck. There is a peripheral lobulated hyperintense component (arrows) and an internal hypointense area (*) that may reflect chronic hemorrhage. **(b, c)** Axial diffusion-weighted **(b)** and ADC **(c)** images show restricted diffusion in the peripheral solid component (arrows). * in **b** = central component. **(d)** Graph from volumetric determination shows that the ADC of the solid component is 0.6 × 10^{-3} mm^2/sec with a high and sharp ADC histogram. **(e)** Axial contrast-enhanced fat-suppressed T1-weighted image shows intense peripheral enhancement of the mass (arrows) with no enhancement of the more central component (*), which owing to its low signal intensity on the T2-weighted image likely represents hemorrhage.

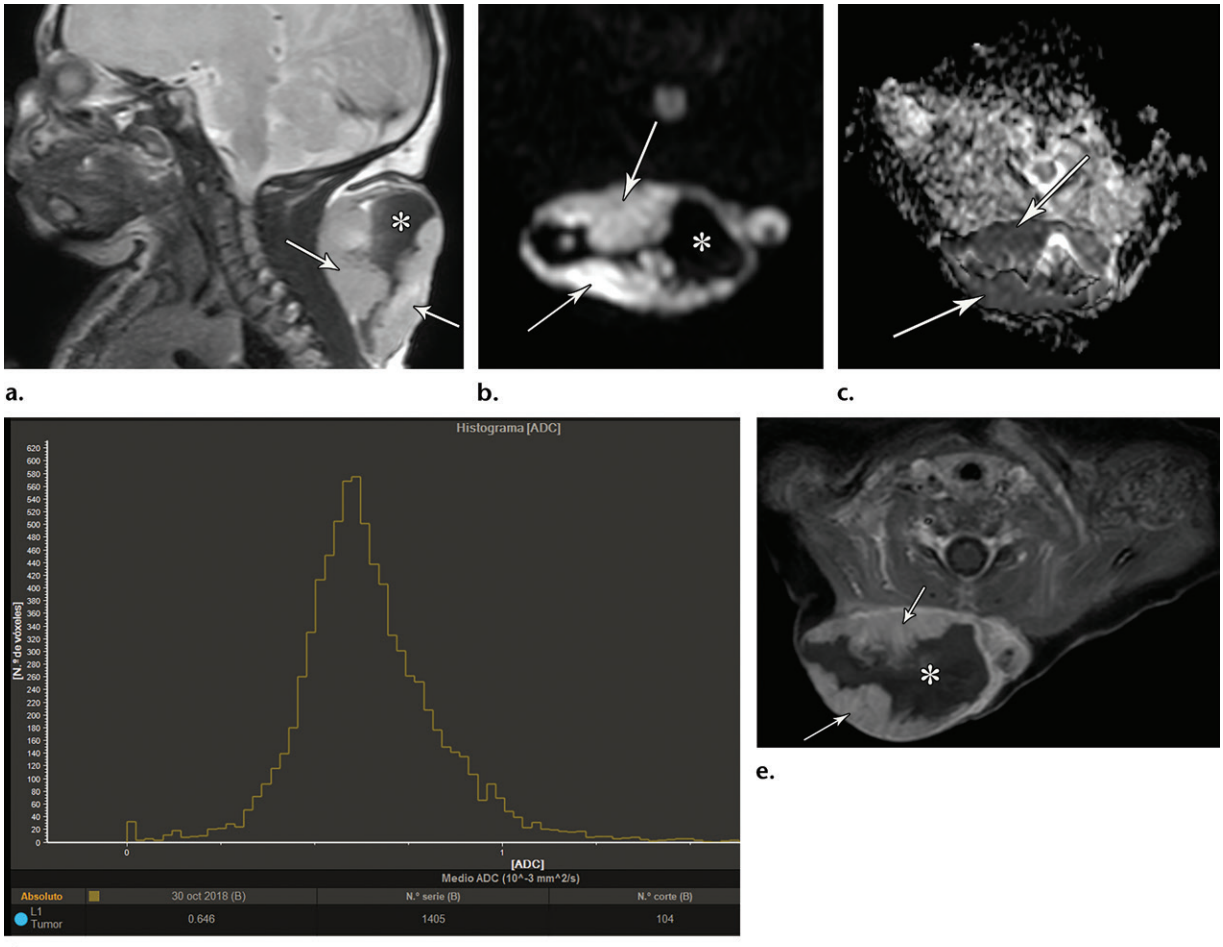

may manifest in early infancy or late childhood (76,77). It most frequently arises in the central nervous system, where it is also called atypical teratoid/rhabdoid tumor (78). It can also occur in the soft tissues of the trunk and mediastinum (76,77).

Unlike with rhabdoid tumor involving the central nervous system, there is scarce literature on soft-tissue rhabdoid tumor. Most of the available descriptions are based on case reports, except for a series of nine well-documented cases described by Garcés-Iñigo et al (78).

Clinical Features.—As with other soft-tissue sarcomas, the clinical manifestation varies depending on the site of origin. Owing to its rapid growth, it may manifest as signs of compression of the surrounding structures (76).

Histopathologic Findings.—The most characteristic appearance is the presence of rhabdoid cells with large eccentric nuclei, prominent nucleoli, and abundant cytoplasm (79). Rhabdoid tumor commonly exhibits necrosis, prominent vascularization, and high mitotic activity. INI1 expression is characteristically lost in extrarenal rhabdoid tumors and is a sensitive marker for these tumors (79).

Conventional MRI Findings.—Extrarenal malignant rhabdoid tumor often manifests as a large heterogeneous mass, hypo- to isointense to muscle on T1-weighted images and heterogeneously hyperintense to muscle on T2-weighted images. In some cases, it may have a cystic central component due to necrosis, reflecting its rapid growth (Fig 14) (78).

Multiparametric MRI Findings.—At DWI, solid areas show diffusion restriction. At DCE MRI, the tumor shows solid areas of avid heterogeneous enhancement that correlate with a type

III or IV curve profile and areas of low signal intensity corresponding to necrosis, which correlate with a type I curve profile. The tumor can be locally aggressive, invading surrounding structures (78).

Treatment.—Treatment includes radiation therapy in all patients after a combination of chemotherapy and surgery, depending on the location of the tumor. However, the prognosis is poor, and the survival rate at 5 years is less than 50% regardless of the therapy used (76).

Conclusion

Use of conventional MRI together with multiparametric MRI techniques provides additional data for detection, characterization, and staging of soft-tissue sarcomas and for follow-up during and after treatment. Advanced multiparametric MRI may have prognostic value in predicting patient response to preoperative neoadjuvant treatment and also in evaluating residual disease after surgery.

Rhabdomyosarcoma is the most frequent soft-tissue sarcoma in children, with the embryonal type being the most prevalent and with a better prognosis. MPNST often manifests as peripheral nodular enhancement and intratumor necrosis, which are not typical in neurofibromas. Synovial sarcoma is the second most common soft-tissue sarcoma in children and may demonstrate the triple signal intensity sign on T2-weighted images, which is highly suggestive of this entity. Extraosseous Ewing sarcoma may exhibit high-flow feeding vessels, although this finding is not specific.

As a general rule, soft-tissue sarcomas usually manifest with restricted diffusion and a type III or IV curve profile. In the presence of internal necrosis and cystic component, the associated curve profile is type I. Fibrosis and granulation tissue usually display a type V curve profile.

Disclosures of Conflicts of Interest.—**J.M.d.C.** *Activities related to the present article:* disclosed no relevant relationships. *Activities not related to the present article:* speaker for Guerbet. *Other activities:* disclosed no relevant relationships.

References

1. Fletcher CDM, Bridge JA, Hogendoorn PCW, Mertens F, eds. WHO classification of tumours of soft tissue and bone. Lyon, France: IARC, 2013.
2. Ferrari A, Sultan I, Huang TT, et al. Soft tissue sarcoma across the age spectrum: a population-based study from the Surveillance Epidemiology and End Results database. Pediatr Blood Cancer 2011;57(6):943–949.
3. Vilanova JC. WHO Classification of Soft Tissue Tumors. In: Vanhoenacker FM, Parizel PM, Gielen JL, eds. Imaging of Soft Tissue Tumors. Heidelberg, Germany: Springer, 2017; 187–196.
4. Vilanova JC, Baleato-Gonzalez S, Romero MJ, Carrascoso-Arranz J, Luna A. Assessment of Musculoskeletal Malignancies with Functional MR Imaging. Magn Reson Imaging Clin N Am 2016;24(1):239–259.
5. Schoot RA, McHugh K, van Rijn RR, et al. Response assessment in pediatric rhabdomyosarcoma: can Response Evaluation Criteria in Solid Tumors replace three-dimensional volume assessments? Radiology 2013;269(3):870–878.
6. Laor T. MR imaging of soft tissue tumors and tumor-like lesions. Pediatr Radiol 2004;34(1):24–37.
7. Fayad LM, Jacobs MA, Wang X, Carrino JA, Bluemke DA. Musculoskeletal tumors: how to use anatomic, functional, and metabolic MR techniques. Radiology 2012;265(2):340–356.
8. Orsatti G, Beltrame V, Crimì F, Frigo AC, Bisogno G, Stramare R. Radiologic response assessment in pediatric soft tissue sarcoma: computed-assisted volume evaluation. J Pediatr 2017;182:327–334.e2.
9. Sheybani EF, Eutsler EP, Navarro OM. Fat-containing soft-tissue masses in children. Pediatr Radiol 2016;46(13):1760–1773.
10. Laffan EE, Ngan BY, Navarro OM. Pediatric soft-tissue tumors and pseudotumors: MR imaging features with pathologic correlation. II. Tumors of fibroblastic/myofibroblastic, so-called fibrohistiocytic, muscular, lymphomatous, neurogenic, hair matrix, and uncertain origin. RadioGraphics 2009;29(4):e36.
11. Chhabra A, Ashikyan O, Slepicka C, et al. Conventional MR and diffusion-weighted imaging of musculoskeletal soft tissue malignancy: correlation with histologic grading. Eur Radiol 2019;29(8):4485–4494.
12. Hong JH, Jee WH, Jung CK, Jung JY, Shin SH, Chung YG. Soft tissue sarcoma: adding diffusion-weighted imaging improves MR imaging evaluation of tumor margin infiltration. Eur Radiol 2019;29(5):2589–2597.
13. Subhawong TK, Jacobs MA, Fayad LM. Diffusion-weighted MR imaging for characterizing musculoskeletal lesions. RadioGraphics 2014;34(5):1163–1177.
14. Costa FM, Martins PH, Canella C, Lopes FPPL. Multiparametric MR Imaging of Soft Tissue Tumors and Pseudotumors. Magn Reson Imaging Clin N Am 2018;26(4):543–558.
15. Subhawong TK, Wilky BA. Value added: functional MR imaging in management of bone and soft tissue sarcomas. Curr Opin Oncol 2015;27(4):323–331.
16. Surov A, Nagata S, Razek AA, Tirumani SH, Wienke A, Kahn T. Comparison of ADC values in different malignancies of the skeletal musculature: a multicentric analysis. Skeletal Radiol 2015;44(7):995–1000.
17. Nakajo M, Fukukura Y, Hakamada H, et al. Whole-tumor apparent diffusion coefficient (ADC) histogram analysis to differentiate benign peripheral neurogenic tumors from soft tissue sarcomas. J Magn Reson Imaging 2018;48(3):680–686.
18. Singer AD, Pattany PM, Fayad LM, Tresley J, Subhawong TK. Volumetric segmentation of ADC maps and utility of standard deviation as measure of tumor heterogeneity in soft tissue tumors. Clin Imaging 2016;40(3):386–391.
19. Soldatos T, Ahlawat S, Montgomery E, Chalian M, Jacobs MA, Fayad LM. Multiparametric assessment of treatment response in high-grade soft-tissue sarcomas with anatomic and functional MR imaging sequences. Radiology 2016;278(3):831–840.
20. Fayad LM, Mugera C, Soldatos T, Flammang A, del Grande F. Technical innovation in dynamic contrast-enhanced magnetic resonance imaging of musculoskeletal tumors: an MR angiographic sequence using a sparse k-space sampling strategy. Skeletal Radiol 2013;42(7):993–1000.
21. Lavini C, Buiter MS, Maas M. Use of dynamic contrast enhanced time intensity curve shape analysis in MRI: theory and practice. Rep Med Imaging 2013;6:71–82.
22. van Rijswijk CS, Geirnaerdt MJ, Hogendoorn PC, et al. Soft-tissue tumors: value of static and dynamic gadopentetate dimeglumine–enhanced MR imaging in prediction of malignancy. Radiology 2004;233(2):493–502.
23. Weiss AR, Lyden ER, Anderson JR, et al. Histologic and clinical characteristics can guide staging evaluations for children and adolescents with rhabdomyosarcoma: a report from the Children's Oncology Group Soft Tissue Sarcoma Committee. J Clin Oncol 2013;31(26):3226–3232.

24. Córdoba Rovira SM, Inarejos Clemente EJ. Childhood rhabdomyosarcoma. Radiologia (Madr) 2016;58(6): 481–490.
25. Salem B, Hofherr S, Turner J, Doros L, Smpokou P. Childhood rhabdomyosarcoma in association with a RASopathy clinical phenotype and mosaic germline SOS1 duplication. J Pediatr Hematol Oncol 2016;38(8):e278–e282.
26. Yang P, Grufferman S, Khoury MJ, et al. Association of childhood rhabdomyosarcoma with neurofibromatosis type I and birth defects. Genet Epidemiol 1995;12(5):467–474.
27. Rodjan F, Graaf Pd, Brisse HJ, et al. Second cranio-facial malignancies in hereditary retinoblastoma survivors previously treated with radiation therapy: clinic and radiologic characteristics and survival outcomes. Eur J Cancer 2013;49(8):1939–1947.
28. Häußler SM, Stromberger C, Olze H, Seifert G, Knopke S, Böttcher A. Head and neck rhabdomyosarcoma in children: a 20-year retrospective study at a tertiary referral center. J Cancer Res Clin Oncol 2018;144(2):371–379.
29. Agrons GA, Wagner BJ, Lonergan GJ, Dickey GE, Kaufman MS. Genitourinary rhabdomyosarcoma in children: radiologic-pathologic correlation. RadioGraphics 1997;17(4):919–937.
30. Kitagawa N, Aida N. Biliary rhabdomyosarcoma. Pediatr Radiol 2007;37(10):1059.
31. Kırlı EA, Parlak E, Oğuz B, Talim B, Akçören Z, Karnak İ. Rhabdomyosarcoma of the common bile duct: an unusual cause of obstructive jaundice in a child. Turk J Pediatr 2012;54(6):654–657.
32. Rekhi B, Gupta C, Chinnaswamy G, et al. Clinicopathologic features of 300 rhabdomyosarcomas with emphasis upon differential expression of skeletal muscle specific markers in the various subtypes: a single institutional experience. Ann Diagn Pathol 2018;36:50–60.
33. McCarville MB, Spunt SL, Pappo AS. Rhabdomyosarcoma in pediatric patients: the good, the bad, and the unusual. AJR Am J Roentgenol 2001;176(6):1563–1569.
34. Norman G, Fayter D, Lewis-Light K, McHugh K, Levine D, Phillips B. Mind the gap: extent of use of diffusion-weighted MRI in children with rhabdomyosarcoma. Pediatr Radiol 2015;45(5):778–781.
35. De B, Kinnaman MD, Wexler LH, Kramer K, Wolden SL. Central nervous system relapse of rhabdomyosarcoma. Pediatr Blood Cancer 2018;65(1):e26710.
36. Shah T, Abu-Sanad O, Marsh H. Role of magnetic resonance imaging in the early diagnosis of paratesticular rhabdomyosarcoma. Ann R Coll Surg Engl 2016;98(5):e74–e76.
37. Kobi M, Khatri G, Edelman M, Hines J. Sarcoma botryoides: MRI findings in two patients. J Magn Reson Imaging 2009;29(3):708–712.
38. Bradley JA, Kayton ML, Chi YY, et al. Treatment approach and outcomes in infants with localized rhabdomyosarcoma: a report from the Soft Tissue Sarcoma Committee of the Children's Oncology Group. Int J Radiat Oncol Biol Phys 2019;103(1):19–27.
39. Morotti RA, Nicol KK, Parham DM, et al. An immunohistochemical algorithm to facilitate diagnosis and subtyping of rhabdomyosarcoma: the Children's Oncology Group experience. Am J Surg Pathol 2006;30(8):962–968.
40. Arnold MA, Anderson JR, Gastier-Foster JM, et al. Histology, fusion status, and outcome in alveolar rhabdomyosarcoma with low-risk clinical features: a report from the Children's Oncology Group. Pediatr Blood Cancer 2016;63(4):634–639.
41. van Vliet M, Kliffen M, Krestin GP, van Dijke CF. Soft tissue sarcomas at a glance: clinical, histological, and MR imaging features of malignant extremity soft tissue tumors. Eur Radiol 2009;19(6):1499–1511.
42. Stein-Wexler R. Pediatric soft tissue sarcomas. Semin Ultrasound CT MR 2011;32(5):470–488.
43. Ferrari A, Bleyer A, Patel S, Chiaravalli S, Gasparini P, Casanova M. The challenge of the management of adolescents and young adults with soft tissue sarcomas. Pediatr Blood Cancer 2018;65(7):e27013.
44. Dangoor A, Seddon B, Gerrand C, Grimer R, Whelan J, Judson I. UK guidelines for the management of soft tissue sarcomas. Clin Sarcoma Res 2016;6(1):20.
45. Winter S, Fasola S, Brisse H, Mosseri V, Orbach D. Relapse after localized rhabdomyosarcoma: evaluation of the efficacy of second-line chemotherapy. Pediatr Blood Cancer 2015;62(11):1935–1941.
46. Reilly KM, Kim A, Blakely J, et al. Neurofibromatosis type 1–associated MPNST state of the science: outlining a research agenda for the future. J Natl Cancer Inst 2017;109(8).
47. Wasa J, Nishida Y, Tsukushi S, et al. MRI features in the differentiation of malignant peripheral nerve sheath tumors and neurofibromas. AJR Am J Roentgenol 2010;194(6): 1568–1574.
48. Pekmezci M, Reuss DE, Hirbe AC, et al. Morphologic and immunohistochemical features of malignant peripheral nerve sheath tumors and cellular schwannomas. Mod Pathol 2015;28(2):187–200.
49. Prieto-Granada CN, Wiesner T, Messina JL, Jungbluth AA, Chi P, Antonescu CR. Loss of H3K27me3 expression is a highly sensitive marker for sporadic and radiation-induced MPNST. Am J Surg Pathol 2016;40(4):479–489.
50. Li CS, Huang GS, Wu HD, et al. Differentiation of soft tissue benign and malignant peripheral nerve sheath tumors with magnetic resonance imaging. Clin Imaging 2008;32(2):121–127.
51. Matsumine A, Kusuzaki K, Nakamura T, et al. Differentiation between neurofibromas and malignant peripheral nerve sheath tumors in neurofibromatosis 1 evaluated by MRI. J Cancer Res Clin Oncol 2009;135(7):891–900.
52. Soldatos T, Fisher S, Karri S, Ramzi A, Sharma R, Chhabra A. Advanced MR imaging of peripheral nerve sheath tumors including diffusion imaging. Semin Musculoskelet Radiol 2015;19(2):179–190.
53. Gottumukkala RV, Gee MS, Hampilos PJ, Greer MC. Current and emerging roles of whole-body MRI in evaluation of pediatric cancer patients. RadioGraphics 2019;39(2): 516–534.
54. Valentin T, Le Cesne A, Ray-Coquard I, et al. Management and prognosis of malignant peripheral nerve sheath tumors: the experience of the French Sarcoma Group (GSF-GETO). Eur J Cancer 2016 March;56:77–84.
55. Ferrari A, De Salvo GL, Brennan B, et al. Synovial sarcoma in children and adolescents: the European Pediatric Soft Tissue Sarcoma Study Group prospective trial (EpSSG NRSTS 2005). Ann Oncol 2015;26(3):567–572.
56. Speth BM, Krieg AH, Kaelin A, et al. Synovial sarcoma in patients under 20 years of age: a multicenter study with a minimum follow-up of 10 years. J Child Orthop 2011;5(5):335–342.
57. Bixby SD, Hettmer S, Taylor GA, Voss SD. Synovial sarcoma in children: imaging features and common benign mimics. AJR Am J Roentgenol 2010;195(4):1026–1032.
58. Jones BC, Sundaram M, Kransdorf MJ. Synovial sarcoma: MR imaging findings in 34 patients. AJR Am J Roentgenol 1993;161(4):827–830.
59. Thway K, Fisher C. Synovial sarcoma: defining features and diagnostic evolution. Ann Diagn Pathol 2014;18(6): 369–380.
60. Murphey MD, Gibson MS, Jennings BT, Crespo-Rodríguez AM, Fanburg-Smith J, Gajewski DA. Imaging of synovial sarcoma with radiologic-pathologic correlation. RadioGraphics 2006;26(5):1543–1565.
61. van Rijswijk CS, Hogendoorn PC, Taminiau AH, Bloem JL. Synovial sarcoma: dynamic contrast-enhanced MR imaging features. Skeletal Radiol 2001;30(1):25–30.
62. Scheer M, Dantonello T, Hallmen E, et al. Synovial sarcoma recurrence in children and young adults. Ann Surg Oncol 2016;23(suppl 5):618–626.
63. Lahl M, Fisher VL, Laschinger K. Ewing's sarcoma family of tumors: an overview from diagnosis to survivorship. Clin J Oncol Nurs 2008;12(1):89–97.
64. Murphey MD, Senchak LT, Mambalam PK, Logie CI, Klassen-Fischer MK, Kransdorf MJ. Ewing sarcoma family of tumors: radiologic-pathologic correlation. RadioGraphics 2013;33(3):803–831.
65. Orr WS, Denbo JW, Billups CA, et al. Analysis of prognostic factors in extraosseous Ewing sarcoma family of tumors: review of St. Jude Children's Research Hospital experience. Ann Surg Oncol 2012;19(12):3816–3822.

66. Edwards TM, Duran MS, Meeker TM. Congenital infantile fibrosarcoma in the premature infant. Adv Neonatal Care 2017;17(6):440–450.
67. Steelman C, Katzenstein H, Parham D, et al. Unusual presentation of congenital infantile fibrosarcoma in seven infants with molecular-genetic analysis. Fetal Pediatr Pathol 2011;30(5):329–337.
68. Farmakis SG, Herman TE, Siegel MJ. Congenital infantile fibrosarcoma. J Perinatol 2014;34(4):329–330.
69. Ainsworth KE, Chavhan GB, Gupta AA, Hopyan S, Taylor G. Congenital infantile fibrosarcoma: review of imaging features. Pediatr Radiol 2014;44(9):1124–1129.
70. Pavlick D, Schrock AB, Malicki D, et al. Identification of NTRK fusions in pediatric mesenchymal tumors. Pediatr Blood Cancer 2017;64(8):e26433.
71. Canale S, Vanel D, Couanet D, Patte C, Caramella C, Dromain C. Infantile fibrosarcoma: magnetic resonance imaging findings in six cases. Eur J Radiol 2009;72(1):30–37.
72. Hanna SL, Kaste S, Jenkins JJ, et al. Epithelioid sarcoma: clinical, MR imaging and pathologic findings. Skeletal Radiol 2002;31(7):400–412.
73. Sakurai T, Kusumoto H, Wakasa T, Ohta Y, Konishi E, Shiono H. Epithelioid sarcoma in the chest wall: a case report and literature review. Surg Case Rep 2018;4(1):77.
74. Modena P, Lualdi E, Facchinetti F, et al. SMARCB1/INI1 tumor suppressor gene is frequently inactivated in epithelioid sarcomas. Cancer Res 2005;65(10):4012–4019.
75. Beckwith JB, Palmer NF. Histopathology and prognosis of Wilms tumors: results from the First National Wilms' Tumor Study. Cancer 1978;41(5):1937–1948.
76. Orbach D, Rey A, Oberlin O, et al. Soft tissue sarcoma or malignant mesenchymal tumors in the first year of life: experience of the International Society of Pediatric Oncology (SIOP) Malignant Mesenchymal Tumor Committee. J Clin Oncol 2005;23(19):4363–4371.
77. Perlman EJ, Ali SZ, Robinson R, Lindato R, Griffin CA. Infantile extrarenal rhabdoid tumor. Pediatr Dev Pathol 1998;1(2):149–152.
78. Garcés-Iñigo EF, Leung R, Sebire NJ, McHugh K. Extrarenal rhabdoid tumours outside the central nervous system in infancy. Pediatr Radiol 2009;39(8):817–822.
79. Kreiger PA, Judkins AR, Russo PA, et al. Loss of INI1 expression defines a unique subset of pediatric undifferentiated soft tissue sarcomas. Mod Pathol 2009;22(1):142–150.